# Semi-Lagrangian Vlasov-Poisson solvers with a strong external uniform magnetic field

Anh-Tuan Vu, Michel Mehrenberger

# Semi-Lagrangian Vlasov-Poisson solvers with a strong external uniform magnetic field

Michel MEHRENBERGER [*], Anh-Tuan VU [†]

(December 5, 2023)

**Abstract**

In this article, we numerically solve the long-time Vlasov-Poisson system with a strong external magnetic field. For that, we consider a backward semi-Lagrangian method as follows: we first propose an approximation of the characteristics based on first and second order explicit numerical schemes; then, a 4-D interpolation is performed to update a numerical unknown. We show that when the magnitude of the external magnetic field becomes large while the time step is independent of the fast oscillation in time, this scheme is able to provide a consistent semi-Lagrangian discretization of the guiding center model. In order to avoid 4-D interpolation, we apply a splitting scheme suited for strong magnetic field which is inspired by J. Ameres [1] but uses the semi-Lagrangian solver instead of a Fourier spectral discretization solver. Finally, we present some numerical simulations to validate the capabilities and limits of the methods under the Kelvin-Helmholtz instability test case.

**Keywords:** Vlasov-Poisson system, Guiding-center model, Semi-Lagrangian method, Asymptotic analysis, Splitting schemes.

## 1 Introduction

We consider in this work the 2-D×2-D long-time Vlasov-Poisson equation with a strong uniform external magnetic field

$$\begin{cases} \varepsilon\partial_t f_\varepsilon + v\cdot\nabla_x f_\varepsilon + \dfrac{q}{m}E_\varepsilon\cdot\nabla_v f_\varepsilon + \dfrac{\omega_c}{\varepsilon}{}^\perp v\cdot\nabla_v f_\varepsilon = 0, \quad (t,x,v)\in ]0,T]\times\mathbb{R}^2\times\mathbb{R}^2, \\ E_\varepsilon(t,x) = -\nabla_x\Phi_\varepsilon(t,x),\ -\epsilon_0\Delta_x\Phi_\varepsilon(t,x) = q\rho_\varepsilon(t,x) = q\int_{\mathbb{R}^2} f_\varepsilon(t,x,v)\mathrm{d}v, \\ f_\varepsilon(0,x,v) = f_0(x,v), \end{cases} \tag{1}$$

where the notation ${}^\perp(\cdot)$ stands for the rotation of angle $-\pi/2$, *i.e.*, ${}^\perp v = \mathcal{R}(-\pi/2)v = (v_2,-v_1)$, $v=(v_1,v_2)\in\mathbb{R}^2$. The unknown of the Vlasov equation $f_\varepsilon = f_\varepsilon(t,x,v)$ over the phase space, depending on the time $t\in[0,T]$, the position $x\in\mathbb{R}^2$ and the velocity $v\in\mathbb{R}^2$, represents the distribution of charged particles of mass $m$, charge $q$. The self-consistent electric field $E_\varepsilon$ induced by the particle density $f_\varepsilon$ is determined by the Poisson equation. The term $\frac{\omega_c}{\varepsilon}{}^\perp v$, where $\omega_c = \frac{qB}{m}$ denotes the cyclotron frequency, corresponds to the projection of the magnetic force in the plane orthogonal to the magnetic field. The given parameter

[*]Aix Marseille Université, CNRS, Centrale Marseille, Institut de Mathématiques de Marseille, UMR 7373, Château Gombert 39 rue F. Joliot Curie, 13453 Marseille FRANCE. E-mail : michel.MEHRENBERGER@univ-amu.fr

[†]Aix Marseille Université, CNRS, Centrale Marseille, Institut de Mathématiques de Marseille, UMR 7373, Château Gombert 39 rue F. Joliot Curie, 13453 Marseille FRANCE. E-mail : anh-tuan.vu@univ-amu.fr

$\varepsilon > 0$ is inversely proportional to the strength of the magnetic field. As $\varepsilon \to 0$, it can be proved (see [18, 16]), that the particle density $(\rho_\varepsilon)_{\varepsilon>0}$ converges in some ways to the unique solution $\rho$ of the guiding center model

$$\begin{cases} \partial_t \rho(t,x) + \dfrac{^\perp E(t,x)}{B} \cdot \nabla_x \rho(t,x) = 0, \ (t,x) \in ]0,T] \times \mathbb{R}^2, \\ E(t,x) = -\nabla_x \Phi(t,x), \ -\epsilon_0 \Delta_x \Phi(t,x) = q\rho(t,x), \\ \rho(0,x) = \int_{\mathbb{R}^2} f_0(x,v)\mathrm{d}v. \end{cases} \tag{2}$$

The guiding center model is the non-linear two-dimensional transport equation that describes the electric cross field drift $\frac{^\perp E}{B}$ in the plane orthogonal to the magnetic field direction.

In this work, we perform the numerical solution of the Vlasov-Poisson system by backward semi-Lagrangian (BSL) methods which are very popular in solving the kinetic equation (see [11, 12, 19]). They can be viewed as a combination of Lagrangian (which consider macro-particles moving according to the characteristics) and Eulerian (which look at values of the unknown on a phase space grid) methods. By making use of the invariance of the distribution function along the trajectories, semi-Lagrangian methods do not need the stability conditions on the time step: time step is only constrained by the physical dynamics that has to be captured. The trajectories of these particles are computed from the characteristic curves of the Vlasov equation

$$\begin{cases} \dfrac{\mathrm{d}X_\varepsilon(t)}{\mathrm{d}t} = \dfrac{1}{\varepsilon} V_\varepsilon(t), & X_\varepsilon(0) = x, \\ \dfrac{\mathrm{d}V_\varepsilon(t)}{\mathrm{d}t} = \dfrac{q}{m} \dfrac{E_\varepsilon(t, X_\varepsilon(t))}{\varepsilon} + \dfrac{\omega_c}{\varepsilon^2} {}^\perp V_\varepsilon(t), & V_\varepsilon(0) = v, \end{cases} \tag{3}$$

where $(X_\varepsilon(t), V_\varepsilon(t))$ represent the position and velocity at time $t$. The main contribution of this paper is to propose a numerical scheme for solving (1) by computing an approximation of the characteristics equations (3) when the parameter $\varepsilon$ vanishes.

Semi-Lagrangian methods have been devoted to the numerical simulation for the Vlasov-Poisson model in the different regimes of plasma physics applications. In [2], an asymptotically stable BSL scheme is performed in the quasi-neutre limit relying on a reformulation of the Poisson equation. For the Vlasov-Poisson equation modeling charged particles in a beam submitted to a highly oscillatory external electric field, a two-scale BSL in [17] and a uniformly accurate forward semi-Lagrangian in [9] have been proposed.

For understanding the effects of strong magnetic fields, let us consider the motion of individual charged particles under the action of a constant electromagnetic field $(E, B)$. The corresponding characteristic curves that satisfy (3) can be explicitly expressed as follows:

$$\begin{cases} V_\varepsilon(t) = \mathcal{R}\left(-\dfrac{\omega_c}{\varepsilon^2} t\right) V_\varepsilon(0) + \varepsilon \left[ I_2 - \mathcal{R}\left(-\dfrac{\omega_c}{\varepsilon^2} t\right) \right] \dfrac{^\perp E}{B}, \\ X_\varepsilon(t) = \underbrace{\left[ X_\varepsilon(0) + \varepsilon \dfrac{^\perp V_\varepsilon(0)}{\omega_c} \right]}_{\text{guiding center}} + \underbrace{t \dfrac{^\perp E}{B}}_{\text{slow drift}} + \underbrace{\mathcal{R}\left(-\dfrac{\omega_c}{\varepsilon^2} t + \pi/2\right) \varepsilon \dfrac{V_\varepsilon(0)}{\omega_c}}_{\text{fast Larmor rotation}} + \mathcal{O}(\varepsilon^2). \end{cases} \tag{4}$$

Therefore, when the charged particles are subject to a strong magnetic field, *i.e.*, $\varepsilon \to 0$, the solution $f_\varepsilon(t,x,v)$ of the Vlasov equation will exhibit fast oscillations in time with wavelength $\mathcal{O}(\varepsilon^2)$. Due to high oscillations in time, if one wants to do accurate simulations of the Vlasov equation using classical numerical schemes, one needs small time steps, typically smaller than $\mathcal{O}(\varepsilon^2)$ in order to fully resolve the oscillations wavelength which leads to prohibitive time computations in the asymptotic regime.

From the discrete point of view, we are interested in a method which is able to capture this singularly oscillatory limit, while the numerical parameters may be kept independent with

respect to $\mathcal{O}(\varepsilon^2)$, in particular the large time step, so that the numerical method provides a consistent discretization of the limit system as $\varepsilon \to 0$. This concept is called Asymptotic Preserving property (see [15]). Several numerical methods of passage from the Vlasov-Poisson system (1) to the guiding center model (2), satisfying this property, have been explored in recent works within the Particle-In-Cell (PIC) method framework (see [6]). This method allows for a focused exploration of constructing a numerical scheme in time for the characteristic equations. Readers can refer to various multi-scale techniques that have been proposed such as the exponential integrator in velocity in [14], implicit-explicit time discretizations in [13], and two-scale formulation integrator in [10].

In this paper, we aim to develop numerical schemes that enable direct simulations of system (1) with large time steps with respect to $\mathcal{O}(\varepsilon^2)$ under the framework of BSL methods. It's worth noting that the multiscale techniques of PIC Vlasov-Poisson solvers in the above mentioned methods can be adapted to the semi-Lagrangian Vlasov-Poisson solver, as both methods involve solving the characteristic equations when $\varepsilon$ becomes small. Here, our initial focus is on constructing explicit numerical methods to solve (3). The primary challenge in solving these ordinary differential equations lies in the stiff term $1/\varepsilon^2$ in the velocity equation, necessitating the use of very small time steps in the standard numerical schemes. Our approach to addressing the stiffness of equations in (3) relies on the formulae (4), where the stiff term $1/\varepsilon^2$ is exactly solved, and the nonlinear term of the electric field is provided at the previous time step. This approach could prove beneficial for the PIC method in solving (1). Subsequently, a 4-D interpolation is performed to evaluate the new value of the distribution function on the grid nodes. However, high-dimensional interpolation is known to be non conservative and it is obviously more demanding in terms of complexity and time. For this reason, splitting methods are very competitive as they simplify the problem into very simple linear transport equations that can be efficiently solved with BSL methods.

To avoid using the high-dimensional interpolation, following [1], we consider the Scovel splitting for the Vlasov equation that means:

$$\varepsilon \partial_t f_\varepsilon + v \cdot \nabla_x f_\varepsilon + \frac{\omega_c}{\varepsilon}^\perp v \cdot \nabla_v f_\varepsilon = 0, \tag{5}$$

$$\varepsilon \partial_t f_\varepsilon + \frac{q}{m} E_\varepsilon(t,x) \cdot \nabla_v f_\varepsilon = 0. \tag{6}$$

Each equation can be solved exactly in time using the characteristic equations when the magnetic field is uniform. Consequently, the numerical error is only due to the splitting in time and the phase space discretization of the distribution function. Then, we introduce an exact splitting strategy to deal with the characteristics associated with (5). Therefore, using the BSL method only requires one dimensional interpolations instead of a high-dimensional interpolation as we could expect. Additionally, a simple parallelization can be performed by distributing the computation on the processors to the values of the variable which is just a parameter.

The fully explicit time discretization techniques for non-splitting BSL simulations will be employed for the Vlasov-Poisson system (1) in the presence of a non-uniform magnetic field. Nevertheless, addressing this aspect falls outside the scope of the current work and is intended for future investigation.

Finally, we shall test the performance of all schemes within the semi-Lagrangian method for a wide range of $\varepsilon$. Our numerical results highlight the robustness of the numerical scheme for the non-splitting semi-Lagrangian solver when using large time steps compared to the fast oscillations in time. It exhibits uniform performance in the limit regime of $\varepsilon$. However, as high-dimensional interpolations in the phase space grid are required at each time step, this may introduce potential numerical diffusions. Therefore, to capture the correct long-time dynamics of the Vlasov-Poisson equation in the highly oscillatory limit regime, the phase space

grid should not be chosen excessively coarse due to spatial errors. Additionally, we show that this method is asymptotic preserving, meaning that it is consistent with the guiding center model as $\varepsilon \to 0$. In contrast, the splitting semi-Lagrangian solver yields incorrect results in the limit regime of $\varepsilon$. Nevertheless, in the intermediate regime of $\varepsilon$, numerical results confirm the scheme's favorable behavior, even with a coarse mesh, highlighting its advantages in terms of CPU time costs and the simplicity of the numerical scheme within the semi-Lagrangian method framework.

Our paper is organized as follows. In Section 2, we first briefly recall the main steps of the semi-Lagrangian method for solving the Vlasov-Poisson system, and then we present time discretization schemes. Section 3 is devoted to the use of two splitting schemes for the Vlasov solution: the Scovel method and the exponential Boris algorithm. Finally, in Section 4, we present numerical simulations using the Kelvin-Helmholtz instability test case.

## 2 Four-dimensional case

The numerical schemes described in the following parts are proposed in the framework of a BSL method. We will now recall the principles of the BSL method for the Vlasov-Poisson system (1) (see [19]) in four dimensions of the phase space. Let's assume that we know the value of $f_\varepsilon$ at time $t^n = n\Delta t$ on the mesh points, where $\Delta t$ stands for the time step. The characteristic curves backward in time corresponding to the Vlasov equation in the system (1) are the solutions of the following first order differential system over the time interval $[t^n, t^{n+1}]$:

$$\begin{cases} \dfrac{\mathrm{d}X_\varepsilon(t;t^{n+1},x,v)}{\mathrm{d}t} = \dfrac{1}{\varepsilon}V_\varepsilon(t;t^{n+1},x,v), \\ \dfrac{\mathrm{d}V_\varepsilon(t;t^{n+1},x,v)}{\mathrm{d}t} = \dfrac{\omega_c}{\varepsilon^2}{}^{\perp}V_\varepsilon(t;t^{n+1},x,v) + \dfrac{1}{\varepsilon}\dfrac{q}{m}E_\varepsilon(t,X_\varepsilon(t;t^{n+1},x,v)), \end{cases} \tag{7}$$

with the initial conditions

$$X_\varepsilon(t^{n+1};t^{n+1},x,v) = x, \quad V_\varepsilon(t^{n+1};t^{n+1},x,v) = v.$$

We denote by $(X_\varepsilon(t;t^{n+1},x,v), V_\varepsilon(t;t^{n+1},x,v))$ the position in phase space at the time $t$, of a particle which was in $(x,v)$ at time $t^{n+1}$. Then, the solution of the Vlasov equation at time $t^{n+1}$ is given by

$$f_\varepsilon(t^{n+1},x,v) = f_\varepsilon(t, X_\varepsilon(t;t^{n+1},x,v), V_\varepsilon(t;t^{n+1},x,v)). \tag{8}$$

Replacing $t$ by $t^n$ in (8), and denoting $X_\varepsilon(t^n;t^{n+1}) = X_\varepsilon(t^n;t^{n+1},x,v)$ and $V_\varepsilon(t^n;t^{n+1}) = V_\varepsilon(t^n;t^{n+1},x,v)$ for simplicity, we have

$$f_\varepsilon(t^{n+1},x,v) = f_\varepsilon(t^n, X_\varepsilon(t^n;t^{n+1}), V_\varepsilon(t^n;t^{n+1})).$$

For each point of the phase space grid $(x,v)$, the distribution function is updated thanks to the two following steps:

**i.** Find the starting point of the characteristic curves ending at $(x,v)$, which is $X_\varepsilon(t^n;t^{n+1})$ and $V_\varepsilon(t^n;t^{n+1})$ by solving (7).

**ii.** Compute $f_\varepsilon(t^n, X_\varepsilon(t^n;t^{n+1}), V_\varepsilon(t^n;t^{n+1}))$ by the method based on Lagrange interpolation, $f_\varepsilon$ being known only at mesh points at time $t^n$

$$f_\varepsilon(t^{n+1},x,v) = \Pi f_\varepsilon(t^n, X_\varepsilon(t^n;t^{n+1}), V_\varepsilon(t^n;t^{n+1})),$$

where $\Pi$ is the Lagrange interpolation operator.

Concerning the time discretization of the characteristics backward in time of the system (7), we propose an explicit numerical scheme that is accurate when using large time steps compared to fast oscillation. The main difficulty in solving the characteristic equation with explicit numerical schemes arises from the stiff terms $1/\varepsilon^2$ associated with the linear term and $1/\varepsilon$ associated with the nonlinear term which requires the use of a very small time step. Thus, to discretize the velocity equation in (7), we will apply the following the strategy: solving exactly the linear stiff part and then using an explicit approximation for the nonlinear term.

### 2.1 An explicit method for characteristics

We initially detail the explicit method for solving the stiff velocity equation in (7) for various small values of $\varepsilon$. Thus we focus on the following type of of ordinary differential equation (ODE):

$$\frac{\mathrm{d}U_\varepsilon(t)}{\mathrm{d}t} = \frac{F(t,U_\varepsilon(t))}{\varepsilon} + \frac{{}^\perp U_\varepsilon(t)}{\varepsilon^2}, \quad U_\varepsilon(t^{n+1}) = U_\varepsilon^{n+1}, \ t \in [t^n, t^{n+1}[, \tag{9}$$

where ${}^\perp U_\varepsilon = (U_\varepsilon^2, -U_\varepsilon^1)$ with $U_\varepsilon = (U_\varepsilon^1, U_\varepsilon^2) \in \mathbb{R}^2$ and where $F$ represents a nonlinear term playing the role of the electric field. Assuming that the vector field $F$ has been approximated at time $t^n$, we seek an approximation $U_\varepsilon(t)$ for the solution of the equation (9) at time $t$. Multiplying (9) by $\mathcal{R}(\frac{t}{\varepsilon^2})$, we obtain

$$\begin{aligned}\frac{\mathrm{d}}{\mathrm{d}t}\left(\mathcal{R}\left(\frac{t}{\varepsilon^2}\right)U_\varepsilon(t)\right) &= \mathcal{R}\left(\frac{t}{\varepsilon^2}\right)\frac{\mathrm{d}U_\varepsilon(t)}{\mathrm{d}t} + \mathcal{R}\left(\frac{t}{\varepsilon^2}+\frac{\pi}{2}\right)\frac{U_\varepsilon(t)}{\varepsilon^2} \\ &= \mathcal{R}\left(\frac{t}{\varepsilon^2}\right)\frac{F(t,U_\varepsilon(t))}{\varepsilon}.\end{aligned}$$

Integrating this equality between $t^{n+1}$ and $t$ yields

$$U_\varepsilon(t) = \mathcal{R}\left(\frac{t^{n+1}-t}{\varepsilon^2}\right)U_\varepsilon(t^{n+1}) + \frac{1}{\varepsilon}\int_{t^{n+1}}^t \mathcal{R}\left(\frac{s-t}{\varepsilon^2}\right)F(s,U_\varepsilon(s))\mathrm{d}s. \tag{10}$$

The stiff part $1/\varepsilon^2$ in the velocity equation is exactly solved. The next step involves deriving approximations to the integral term in (10). Our technique relies on an explicit formula in which the vector field $F$ is given at the position $U_\varepsilon(t^{n+1})$ at time $t^n$, as follows:

$$\frac{1}{\varepsilon}\int_{t^{n+1}}^t \mathcal{R}\left(\frac{s-t}{\varepsilon^2}\right)F(s,U_\varepsilon(s))\mathrm{d}s \approx \frac{1}{\varepsilon}\int_{t^{n+1}}^t \mathcal{R}\left(\frac{s-t}{\varepsilon^2}\right)\mathrm{d}sF(t^n,U_\varepsilon(t^{n+1})).$$

Note the following properties of the rotation matrix:

$$\varepsilon^2\frac{\mathrm{d}}{\mathrm{d}s}\left[\mathcal{R}\left(\frac{s-t}{\varepsilon^2}-\frac{\pi}{2}\right)\right] = \mathcal{R}\left(\frac{s-t}{\varepsilon^2}\right),$$

since

$$\frac{\mathrm{d}}{\mathrm{d}\theta}\mathcal{R}(\theta-\pi/2) = \left(\frac{\mathrm{d}}{\mathrm{d}\theta}\mathcal{R}(\theta)\right)\mathcal{R}(-\pi/2) = \begin{pmatrix}-\sin(\theta) & -\cos(\theta)\\ \cos(\theta) & -\sin(\theta)\end{pmatrix}\begin{pmatrix}0 & 1\\ -1 & 0\end{pmatrix} = \mathcal{R}(\theta).$$

We deduce that

$$\begin{aligned}\frac{1}{\varepsilon}\int_{t^{n+1}}^t \mathcal{R}\left(\frac{s-t}{\varepsilon^2}\right)\mathrm{d}sF(t^n,U_\varepsilon(t^{n+1})) &= \varepsilon\left[\mathcal{R}\left(-\frac{\pi}{2}\right)-\mathcal{R}\left(\frac{t^{n+1}-t}{\varepsilon^2}-\frac{\pi}{2}\right)\right]F(t^n,U_\varepsilon(t^{n+1})) \\ &= \varepsilon\left[I_2-\mathcal{R}\left(\frac{t^{n+1}-t}{\varepsilon^2}\right)\right]{}^\perp F(t^n,U_\varepsilon(t^{n+1})).\end{aligned}$$

Injecting the previous equality in (10), we get the approximation of $U_\varepsilon$ at time $t \in [t^n, t^{n+1}[$:

$$U_\varepsilon(t) \approx \mathcal{R}\left(\frac{t^{n+1}-t}{\varepsilon^2}\right) U_\varepsilon(t^{n+1}) + \varepsilon \left[I_2 - \mathcal{R}\left(\frac{t^{n+1}-t}{\varepsilon^2}\right)\right] {}^\perp F(t^n, U_\varepsilon(t^{n+1})). \tag{11}$$

**Remark 2.1** *The stiff velocity equation in* (7) *was addressed in [13] using an implicit treatment for the stiff term* $1/\varepsilon^2$ *and an explicit approximation for the nonlinear term. When* $\varepsilon \to 0$*, the numerical solution approaches the correct trajectory and fast fluctuations are somehow filtered. In [14], the approach involves solving the stiff linear part* $1/\varepsilon^2$ *exactly, as shown in* (10) *and deriving suitable approximations for numerically integrating the nonlinear term. They solve the ODEs over one fast period using an explicit high-order solver and then, thanks to* (10)*, they compute an approximation of the solution over a large whole number of periods.*

## 2.2 Numerical schemes

Now, we present numerical schemes for the discretization of the Vlasov-Poisson system (1) using the semi-Lagrangian method. Let $f_\varepsilon^n(\cdot,\cdot)$ and $E_\varepsilon^n(\cdot)$ denote the approximations of $f_\varepsilon(t^n,\cdot,\cdot)$ and $E_\varepsilon(t^n,\cdot)$, respectively. Assume that at time $t^n$, we have known approximations for the distribution $f_\varepsilon^n$ and the electric field $E_\varepsilon^n$.

**First order scheme.** We will apply the explicit scheme discussed in subsection 2.1 to approximate the solutions the characteristic equations backward in time (7), which is $(X_\varepsilon(t^n;t^{n+1}), V_\varepsilon(t^n;t^{n+1}))$ By applying (11) to the second equation in (7), we obtain the velocity approximation at time $t$:

$$\begin{aligned} V_\varepsilon(t;t^{n+1}) &= \mathcal{R}\left(\frac{\omega_c}{\varepsilon^2}(t^{n+1}-t)\right) V_\varepsilon(t^{n+1};t^{n+1}) + \varepsilon\left[I_2 - \mathcal{R}\left(\frac{\omega_c}{\varepsilon^2}(t^{n+1}-t)\right)\right] \frac{{}^\perp E_\varepsilon^n(X_\varepsilon(t^{n+1};t^{n+1}))}{B} \\ &= \mathcal{R}\left(\frac{\omega_c}{\varepsilon^2}(t^{n+1}-t)\right) v + \varepsilon\left[I_2 - \mathcal{R}\left(\frac{\omega_c}{\varepsilon^2}(t^{n+1}-t)\right)\right] \frac{{}^\perp E_\varepsilon^n(x)}{B}. \end{aligned}$$

As for the position equation, we inject the previous expression and subsequently integrate the first equation in (7) over the interval from $t^{n+1}$ to $t$

$$\begin{aligned} X_\varepsilon(t;t^{n+1}) = X_\varepsilon(t^{n+1};t^{n+1}) &+ \frac{1}{\varepsilon}\int_{t^{n+1}}^t \mathcal{R}\left(\frac{\omega_c}{\varepsilon^2}(t^{n+1}-s)\right) v \mathrm{d}s \\ &+ \int_{t^{n+1}}^t \left[I_2 - \mathcal{R}\left(\frac{\omega_c}{\varepsilon^2}(t^{n+1}-s)\right)\right] \mathrm{d}s \frac{{}^\perp E_\varepsilon^n(x)}{B}. \end{aligned}$$

Since

$$\frac{\varepsilon^2}{\omega_c}\frac{\mathrm{d}}{\mathrm{d}s}\mathcal{R}\left(\frac{\omega_c}{\varepsilon^2}(t^{n+1}-s)+\frac{\pi}{2}\right) = \mathcal{R}\left(\frac{\omega_c}{\varepsilon^2}(t^{n+1}-s)\right), \tag{12}$$

it implies the approximation of the position at time $t$

$$\begin{aligned} X_\varepsilon(t;t^{n+1}) = x &+ (t-t^{n+1})\frac{{}^\perp E_\varepsilon^n(x)}{B} \\ &+ \frac{\varepsilon}{\omega_c}\left[\mathcal{R}\left(\frac{\omega_c}{\varepsilon^2}(t^{n+1}-t)+\frac{\pi}{2}\right) - \mathcal{R}\left(\frac{\pi}{2}\right)\right] v \\ &- \frac{\varepsilon^2}{\omega_c}\left[\mathcal{R}\left(\frac{\omega_c}{\varepsilon^2}(t^{n+1}-t)+\frac{\pi}{2}\right) - \mathcal{R}\left(\frac{\pi}{2}\right)\right] \frac{{}^\perp E_\varepsilon^n(x)}{B}. \end{aligned}$$

Then the first order scheme writes for $n \geq 0$:

$$f_\varepsilon^{n+1}(x,v) = \Pi f_\varepsilon^n(X_\varepsilon(t^n;t^{n+1}), V_\varepsilon(t^n;t^{n+1})), \tag{13}$$

where the approximation of characteristic curves at time $t^n$ is given by

$$V_\varepsilon(t^n;t^{n+1}) = \mathcal{R}\left(\frac{\omega_c}{\varepsilon^2}\Delta t\right) v + \varepsilon\left[I_2 - \mathcal{R}\left(\frac{\omega_c}{\varepsilon^2}\Delta t\right)\right]\frac{{}^\perp E_\varepsilon^n(x)}{B}, \tag{14}$$

$$\begin{aligned} X_\varepsilon(t^n;t^{n+1}) = x - \Delta t\frac{{}^\perp E_\varepsilon^n(x)}{B} + \frac{\varepsilon}{\omega_c}\left[\mathcal{R}\left(\frac{\omega_c}{\varepsilon^2}\Delta t + \frac{\pi}{2}\right) - \mathcal{R}\left(\frac{\pi}{2}\right)\right] v \\ - \frac{\varepsilon^2}{\omega_c}\left[\mathcal{R}\left(\frac{\omega_c}{\varepsilon^2}\Delta t + \frac{\pi}{2}\right) - \mathcal{R}\left(\frac{\pi}{2}\right)\right]\frac{{}^\perp E_\varepsilon^n(x)}{B}. \end{aligned} \tag{15}$$

**Remark 2.2** *(Consistency in the limit $\varepsilon \to 0$ for a fixed $\Delta t$)*
*Taking to the limit as $\varepsilon \to 0$ in (14) and (15), we find that $(\varepsilon V_\varepsilon(t^n;t^{n+1}))_{\varepsilon>0}$ converges to zero and $X_\varepsilon(t^n;t^{n+1}) \to Y(t^n;t^{n+1},x)$, where the limit $(Y(t^n;t^{n+1},x))_{n\geq 0}$ corresponds to a first order approximation with respect to $\Delta t$ of the guiding center model proposed by the scheme*

$$\begin{cases} Y(t^n;t^{n+1},x) = x - \Delta t\dfrac{{}^\perp E^n(x)}{B}, \\ Y(t^{n+1};t^{n+1},x) = x. \end{cases}$$

In order to capture the correct long time dynamics of the Vlasov-Poisson system in the highly oscillatory limit regime, such first order scheme is not accurate enough. Consequently, we will introduce a high order time discretization scheme for backward semi-Lagrangian methods.

**Second order scheme.** Now we consider a second order scheme with two steps.

**Step 1**: First, we compute the characteristic curves at time $t^{n+1/2} = t^n + \Delta t/2$, which is $X_\varepsilon(t^{n+1/2};t^{n+1})$ and $V_\varepsilon(t^{n+1/2};t^{n+1})$ by solving (7) with the electric field $E_\varepsilon^n(X_\varepsilon(t^{n+1};t^{n+1})) = E_\varepsilon^n(x)$. In the same way as (14)-(15), we have the approximation of characteristic curves at time $t^{n+1/2}$

$$\begin{cases} V_\varepsilon(t^{n+1/2};t^{n+1}) = \mathcal{R}\left(\dfrac{\omega_c}{\varepsilon^2}\dfrac{\Delta t}{2}\right) v + \varepsilon\left[I_2 - \mathcal{R}\left(\dfrac{\omega_c}{\varepsilon^2}\dfrac{\Delta t}{2}\right)\right]\dfrac{{}^\perp E_\varepsilon^n(x)}{B}, \\ X_\varepsilon(t^{n+1/2};t^{n+1}) = x - \dfrac{\Delta t}{2}\dfrac{{}^\perp E_\varepsilon^n(x)}{B} \\ \qquad\qquad + \dfrac{\varepsilon}{\omega_c}\left[\mathcal{R}\left(\dfrac{\omega_c}{\varepsilon^2}\dfrac{\Delta t}{2} + \dfrac{\pi}{2}\right) - \mathcal{R}\left(\dfrac{\pi}{2}\right)\right] v \\ \qquad\qquad - \dfrac{\varepsilon^2}{\omega_c}\left[\mathcal{R}\left(\dfrac{\omega_c}{\varepsilon^2}\dfrac{\Delta t}{2} + \dfrac{\pi}{2}\right) - \mathcal{R}\left(\dfrac{\pi}{2}\right)\right]\dfrac{{}^\perp E_\varepsilon^n(x)}{B}. \end{cases} \tag{16}$$

Then we compute the value of the distribution function $f_\varepsilon$ at time $t^{n+1/2}$ for each mesh point in the phase space grid

$$f_\varepsilon^{n+1/2}(x,v) = \Pi f_\varepsilon^n(X_\varepsilon(t^{n+1/2};t^{n+1}), V_\varepsilon(t^{n+1/2};t^{n+1})).$$

Finally, we substitute the function $f_\varepsilon^{n+1/2}$ into the Poisson equation to calculate an approximation of $E_\varepsilon$ at time $t^{n+1/2}$.

**Step 2**: Thanks to Step 1, we compute $(X_\varepsilon(t^n;t^{n+1}), V_\varepsilon(t^n;t^{n+1}))$ by solving (7) with the electric field $E_\varepsilon^{n+1/2}(X_\varepsilon(t^{n+1/2};t^{n+1}))$. This means that the integral term between $t^{n+1}$ and $t^n$ in (10) has been approximated as

$$\frac{1}{\varepsilon}\int_{t^{n+1}}^{t^n} \mathcal{R}\left(\frac{s-t}{\varepsilon^2}\right) F(s,U_\varepsilon(s))\mathrm{d}s \approx \frac{1}{\varepsilon}\int_{t^{n+1}}^{t^n} \mathcal{R}\left(\frac{s-t}{\varepsilon^2}\right) \mathrm{d}s F(t^{n+1/2},U_\varepsilon(t^{n+1/2})).$$

Hence, we obtain the approximation of characteristic curves at time $t^n$

$$\left\{\begin{array}{l} V_\varepsilon(t^n;t^{n+1}) = \mathcal{R}\left(\frac{\omega_c}{\varepsilon^2}\Delta t\right) v + \varepsilon\left[I_2 - \mathcal{R}\left(\frac{\omega_c}{\varepsilon^2}\Delta t\right)\right]\frac{{}^\perp E_\varepsilon^{n+1/2}(X_\varepsilon(t^{n+1/2};t^{n+1}))}{B}, \\ X_\varepsilon(t^n;t^{n+1}) = x - \Delta t\frac{{}^\perp E_\varepsilon^{n+1/2}(X_\varepsilon(t^{n+1/2};t^{n+1}))}{B} \\ \qquad\qquad + \frac{\varepsilon}{\omega_c}\left[\mathcal{R}\left(\frac{\omega_c}{\varepsilon^2}\Delta t + \frac{\pi}{2}\right) - \mathcal{R}\left(\frac{\pi}{2}\right)\right] v \\ \qquad\qquad - \frac{\varepsilon^2}{\omega_c}\left[\mathcal{R}\left(\frac{\omega_c}{\varepsilon^2}\Delta t + \frac{\pi}{2}\right) - \mathcal{R}\left(\frac{\pi}{2}\right)\right]\frac{{}^\perp E_\varepsilon^{n+1/2}(X_\varepsilon(t^{n+1/2};t^{n+1}))}{B}. \end{array}\right. \tag{17}$$

Finally, the value of the solution $f_\varepsilon$ at time $t^{n+1}$ is given by a last interpolation

$$f_\varepsilon^{n+1}(x,v) = \Pi f_\varepsilon^n(X_\varepsilon(t^n;t^{n+1}), V_\varepsilon(t^n;t^{n+1})).$$

**Remark 2.3** *(Consistency in the limit $\varepsilon \to 0$ for a fixed $\Delta t$)*
*Passing to the limit as $\varepsilon \to 0$ in* (16), (17) *yields*

$$\left\{\begin{array}{l} Y(t^{n+1/2};t^{n+1},x) = x - \frac{\Delta t}{2}\frac{{}^\perp E^n(x)}{B},\ Y(t^{n+1};t^{n+1},x) = x, \\ Y(t^n;t^{n+1},x) = x - \Delta t\frac{{}^\perp E^{n+1/2}(Y(t^{n+1/2};t^{n+1},x))}{B}, \end{array}\right.$$

*which is a consistent and second order approximation with respect to $\Delta t$ of the guiding center equation.*

**Remark 2.4** *(Filter out the fast rotation around the magnetic field lines)*
*In order to filter out the fast oscillations corresponding to the magnetic field $\frac{\omega_c}{\varepsilon^2}{}^\perp v\cdot\nabla_v$, we perform the change of coordinates*

$$f_\varepsilon(t,x,v) = g_\varepsilon(t,x,w),\ \text{with } w = \mathcal{R}\left(\frac{\omega_c}{\varepsilon^2}t\right) v.$$

*By applying the chain rule, the Vlasov equation in* (1) *becomes:*

$$\partial_t g_\varepsilon + \frac{1}{\varepsilon}\mathcal{R}\left(-\frac{\omega_c}{\varepsilon^2}t\right) w\cdot\nabla_x g_\varepsilon + \frac{1}{\varepsilon}\mathcal{R}\left(\frac{\omega_c}{\varepsilon^2}t\right)\frac{q}{m}E_\varepsilon(t,x)\cdot\nabla_w g_\varepsilon = 0, \tag{18}$$

*with the initial condition $g_\varepsilon(0,x,w) = f_0(x,w)$. The characteristic curves backward in time corresponding to the equation* (18) *are given by:*

$$\left\{\begin{array}{l} \frac{\mathrm{d}X_\varepsilon(t;t^{n+1},x,w)}{\mathrm{d}t} = \frac{1}{\varepsilon}\mathcal{R}\left(-\frac{\omega_c}{\varepsilon^2}t\right) W_\varepsilon(t;t^{n+1},x,w), \\ \frac{\mathrm{d}W_\varepsilon(t;t^{n+1},x,w)}{\mathrm{d}t} = \frac{1}{\varepsilon}\mathcal{R}\left(\frac{\omega_c}{\varepsilon^2}t\right)\frac{q}{m}E_\varepsilon(t,X_\varepsilon(t;t^{n+1},x,w)). \end{array}\right.$$

*The first order numerical scheme writes:*

$$g_\varepsilon^{n+1}(x,w) = \Pi g_\varepsilon^n(X_\varepsilon(t^n;t^{n+1},x,w), W_\varepsilon(t^n;t^{n+1},x,w)),$$

*where $(X_\varepsilon(t^n;t^{n+1},x,w), W_\varepsilon(t^n;t^{n+1},x,w))$ is the approximation of characteristic curves at time $t^n$*

$$\left\{\begin{array}{l} W_\varepsilon(t^n;t^{n+1},x,w) = w + \varepsilon\mathcal{R}\left(\frac{\omega_c}{\varepsilon^2}t^n\right)\left[I_2 - \mathcal{R}\left(\frac{\omega_c}{\varepsilon^2}\Delta t\right)\right]\frac{{}^\perp E_\varepsilon^n(x)}{B}, \\ X_\varepsilon(t^n;t^{n+1},x,w) = x - \Delta t\frac{{}^\perp E_\varepsilon^n(x)}{B} \\ \qquad\qquad + \frac{\varepsilon}{\omega_c}\left[\mathcal{R}\left(-\frac{\omega_c}{\varepsilon^2}t^n + \frac{\pi}{2}\right) - \mathcal{R}\left(-\frac{\omega_c}{\varepsilon^2}t^{n+1} + \frac{\pi}{2}\right)\right] w \\ \qquad\qquad + \frac{\varepsilon^2}{\omega_c}\left[I_2 - \mathcal{R}\left(\frac{\omega_c}{\varepsilon^2}\Delta t\right)\right]\frac{E_\varepsilon^n(x)}{B}. \end{array}\right.$$

*The second order numerical scheme is provided in the same manner as* (16)-(17).

The methods presented in this part give much more accurate results than the previous first order scheme in subsection 2.1. However, it requires one more high interpolation and, consequently, has a higher computational cost. Thus, to reduce the computational complexity, we particularly emphasize the role of directional splitting designed for the backward semi-Lagrangian method.

# 3 Splitting case

## 3.1 A time splitting discretization

We apply the Scovel splitting for the numerical solution of the Vlasov–Poisson system (1) under the BSL method. This splitting, detailed in [1] where a spectral method was used for spatial discretization, operates on the distribution function $f_\varepsilon$ and successively solves equations (5) and (6). The electric field $E_\varepsilon$ is computed from the Poisson equation after solving the equation (5). The characteristic curves backward in time associated with the Scovel method and corresponding to the equations (5) and (6) are expressed respectively:

$$\mathcal{E}_\varepsilon^1(t): \begin{cases} \dfrac{\mathrm{d}X_\varepsilon(t;t^{n+1},x,v)}{\mathrm{d}t} = \dfrac{1}{\varepsilon}V_\varepsilon(t;t^{n+1},x,v), \\ \dfrac{\mathrm{d}V_\varepsilon(t;t^{n+1},x,v)}{\mathrm{d}t} = \dfrac{\omega_c}{\varepsilon^2}{}^{\perp}V_\varepsilon(t;t^{n+1},x,v), \end{cases} \tag{19}$$

$$\mathcal{E}_\varepsilon^2(t): \begin{cases} \dfrac{\mathrm{d}X_\varepsilon(t;t^{n+1},x,v)}{\mathrm{d}t} = 0, \\ \dfrac{\mathrm{d}V_\varepsilon(t;t^{n+1},x,v)}{\mathrm{d}t} = \dfrac{1}{\varepsilon}\dfrac{q}{m}E_\varepsilon(t,X_\varepsilon(t;t^{n+1},x,v)). \end{cases} \tag{20}$$

In the case of a uniform magnetic field, the characteristic curves corresponding to (19) form a linear system and can therefore be solved exactly. Indeed, from (12), the exact solutions of the characteristic curves in (19) are given by:

$$V_\varepsilon(t;t^{n+1}) = \mathcal{R}(\theta)V_\varepsilon(t^{n+1};t^{n+1}) = \mathcal{R}(\theta)v, \;\; \theta = \frac{\omega_c}{\varepsilon^2}(t^{n+1}-t). \tag{21}$$

$$\begin{aligned} X_\varepsilon(t;t^{n+1}) &= X_\varepsilon(t^{n+1};t^{n+1}) + \frac{1}{\varepsilon}\int_{t^{n+1}}^{t} V_\varepsilon(\tau;t^{n+1})\mathrm{d}\tau \\ &= x + \frac{\varepsilon}{\omega_c}\int_{t^{n+1}}^{t}\frac{\mathrm{d}}{\mathrm{d}\tau}\mathcal{R}\left(\frac{\omega_c}{\varepsilon^2}(t^{n+1}-\tau)+\frac{\pi}{2}\right)v\mathrm{d}\tau \\ &= x + \frac{\varepsilon}{\omega_c}\left[\mathcal{R}\left(\frac{\omega_c}{\varepsilon^2}(t^{n+1}-t)+\frac{\pi}{2}\right) - \mathcal{R}\left(\frac{\pi}{2}\right)\right]v \\ &= x + \frac{\varepsilon}{\omega_c}\begin{pmatrix}\sin(-\theta) & 1-\cos(\theta)\\ \cos(\theta)-1 & \sin(-\theta)\end{pmatrix}v, \;\; \theta = \frac{\omega_c}{\varepsilon^2}(t^{n+1}-t). \end{aligned} \tag{22}$$

We can therefore rewrite the equations (21) and (22) in matrix form as follows:

$$\begin{pmatrix} X_\varepsilon(t;t^{n+1}) \\ V_\varepsilon(t;t^{n+1}) \end{pmatrix} = \begin{pmatrix} 1 & 0 & \frac{\varepsilon}{\omega_c}\sin(-\theta) & \frac{\varepsilon}{\omega_c}(1-\cos(\theta)) \\ 0 & 1 & \frac{\varepsilon}{\omega_c}(\cos(\theta)-1) & \frac{\varepsilon}{\omega_c}\sin(-\theta) \\ 0 & 0 & \cos(\theta) & \sin(-\theta) \\ 0 & 0 & \sin(\theta) & \cos(\theta) \end{pmatrix}\begin{pmatrix} x \\ v \end{pmatrix}. \tag{23}$$

We denote $\gamma_\varepsilon^1$ and $\gamma_\varepsilon^2$ as the exact solutions corresponding to the equations (5) and (6) from an initial condition $(f_\varepsilon, E_\varepsilon)$ at time $t = t^n$. The solution $\gamma_\varepsilon^2$ at time $t^{n+1}$ can be computed

exactly in time since the advection field in the equation (6) does not depend on the variable to be advected. Thus, it is given explicitly by

$$\gamma_\varepsilon^2(t^{n+1},x,v) = f_\varepsilon(t^n, X_\varepsilon(t^n;t^{n+1}), V_\varepsilon(t^n;t^{n+1})) = f_\varepsilon(t^n,x,v-\Delta t\frac{q}{m\varepsilon}E_\varepsilon(t^n,x)). \tag{24}$$

As a consequence, we only perform 1-D interpolations instead of 2-D interpolation. On the other hand, from (23), we can deduce the exact solution $\gamma_\varepsilon^1$ of equation (5) at time $t^{n+1}$, expressed as:

$$\gamma_\varepsilon^1(t^{n+1},x,v) = f_\varepsilon(t^n, X_\varepsilon(t^n;t^{n+1}), V_\varepsilon(t^n;t^{n+1})). \tag{25}$$

For the interpolation step, a 4-D interpolation is required to update the function values of the numerical unknown on the phase space grid. Therefore, to avoid this 4-D interpolation, we propose an exact splitting that enables us to reduce it to 1-D interpolations. To achieve this, we first observe that the matrix (23) can be expressed as two shears:

$$\begin{pmatrix} 1 & 0 & 0 & 0 \\ 0 & 1 & 0 & 0 \\ 0 & 0 & \cos(\theta) & \sin(-\theta) \\ 0 & 0 & \sin(\theta) & \cos(\theta) \end{pmatrix} \begin{pmatrix} 1 & 0 & \frac{\varepsilon}{\omega_c}\sin(-\theta) & \frac{\varepsilon}{\omega_c}(1-\cos(\theta)) \\ 0 & 1 & \frac{\varepsilon}{\omega_c}(\cos(\theta)-1) & \frac{\varepsilon}{\omega_c}\sin(-\theta) \\ 0 & 0 & 1 & 0 \\ 0 & 0 & 0 & 1 \end{pmatrix}, \ \theta = \frac{\omega_c}{\varepsilon^2}\Delta t. \tag{26}$$

Then, the first matrix is decomposed into three shears as (31) and the second one can be decomposed into a product of four shear transformations:

$$\begin{pmatrix} 1 & 0 & \frac{\varepsilon}{\omega_c}\sin(-\theta) & 0 \\ 0 & 1 & 0 & 0 \\ 0 & 0 & 1 & 0 \\ 0 & 0 & 0 & 1 \end{pmatrix} \begin{pmatrix} 1 & 0 & 0 & 0 \\ 0 & 1 & \frac{\varepsilon}{\omega_c}(\cos(\theta)-1) & 0 \\ 0 & 0 & 1 & 0 \\ 0 & 0 & 0 & 1 \end{pmatrix} \begin{pmatrix} 1 & 0 & 0 & \frac{\varepsilon}{\omega_c}(1-\cos(\theta)) \\ 0 & 1 & 0 & 0 \\ 0 & 0 & 1 & 0 \\ 0 & 0 & 0 & 1 \end{pmatrix} \begin{pmatrix} 1 & 0 & 0 & 0 \\ 0 & 1 & 0 & \frac{\varepsilon}{\omega_c}\sin(-\theta) \\ 0 & 0 & 1 & 0 \\ 0 & 0 & 0 & 1 \end{pmatrix}$$

leading to the exact splitting in time. Consequently, we only need to solve shear transformations which are nothing but one-dimensional linear advection. Thus, programming with parallel computing becomes quite natural, and the method proves to be very efficient.

**Remark 3.1** *The splitting underlying the exponential Boris algorithm (see [8]) arises from the fact that we divide equation* (5) *into the following two equations:*

$$\varepsilon\partial_t f_\varepsilon + v\cdot\nabla_x f_\varepsilon = 0, \tag{27}$$

$$\varepsilon\partial_t f_\varepsilon + \frac{\omega_c}{\varepsilon}{}^\perp v\cdot\nabla_v f_\varepsilon = 0. \tag{28}$$

*The exact solution* $\gamma_\varepsilon^{1,1}$ *to* (27) *at time* $t^{n+1}$ *from the initial condition* $f_\varepsilon$ *at time* $t^n$ *is given explicitly by*

$$\gamma_\varepsilon^{1,1}(t^{n+1},x,v) = f_\varepsilon(t^n, x-\frac{\Delta t}{\varepsilon}v, v). \tag{29}$$

*The solution* $\gamma_\varepsilon^{1,2}$ *of* (28) *at time* $t^{n+1}$ *can be also solved exactly in time, and it is given by*

$$\gamma_\varepsilon^{1,2}(t^{n+1},x,v) = f_\varepsilon(t^n, X_\varepsilon(t^n;t^{n+1}), V_\varepsilon(t^n;t^{n+1})) = f_\varepsilon(t^n,x,\mathcal{R}(\theta)v), \ \theta = \frac{\omega_c}{\varepsilon^2}\Delta t. \tag{30}$$

*Therefore, during the interpolation step, a 2-D interpolation is necessaryin the variable* $v$ *to update the numerical unknown* $\gamma_\varepsilon^{1,2}$*. However, high-dimensional interpolation is known to be non conservative and it is obviously more demanding in terms of complexity and time. To remedy this difficulty, we use the method in [4], where the authors proposed a splitting strategy to reduce the problem into very simple one-dimensional linear transport equations. These can be solved efficiently with the semi-Lagrangian method. The splitting is based on*

*the fact that the two-dimensional rotation matrix $\mathcal{R}(\theta)$ is decomposed into a product of three shear matrices:*

$$\mathcal{R}(\theta) = \begin{pmatrix} \cos(\theta) & -\sin(\theta) \\ \sin(\theta) & \cos(\theta) \end{pmatrix} = \begin{pmatrix} 1 & -\tan(\theta/2) \\ 0 & 1 \end{pmatrix} \begin{pmatrix} 1 & 0 \\ \sin(\theta) & 1 \end{pmatrix} \begin{pmatrix} 1 & -\tan(\theta/2) \\ 0 & 1 \end{pmatrix}, \tag{31}$$

*for $\theta \neq k\pi, k \in \mathbb{Z}^\star$. This formula has been generalized to arbitrary dimensions, the reader can refer to [3, 5].*

**Remark 3.2** *For the small angle $\theta$, by approximating $\sin(x) \approx x$ and $1 - \cos(x) \approx x^2/2 \approx 0$ in the second matrix of (26), the product of two matrices in (26) becomes*

$$\begin{pmatrix} 1 & 0 & 0 & 0 \\ 0 & 1 & 0 & 0 \\ 0 & 0 & \cos(\theta) & \sin(-\theta) \\ 0 & 0 & \sin(\theta) & \cos(\theta) \end{pmatrix} \begin{pmatrix} 1 & 0 & -\Delta t/\varepsilon & 0 \\ 0 & 1 & 0 & -\Delta t/\varepsilon \\ 0 & 0 & 1 & 0 \\ 0 & 0 & 0 & 1 \end{pmatrix}, \quad \theta = \frac{\omega_c}{\varepsilon^2}\Delta t,$$

*which implies that*

$$\gamma_\varepsilon^1 = \gamma_\varepsilon^{1,2} \circ \gamma_\varepsilon^{1,1},$$

*where $\gamma_\varepsilon^{1,1}$ and $\gamma_\varepsilon^{1,2}$ are exact solutions of equations (27) and (28) respectively. This implies that the Scovel splitting coincides with the exponential Boris algorithm when the following condition on the time step is satisfied:*

$$\Delta t < \mathcal{O}(\varepsilon^2). \tag{32}$$

Regarding the time discretization of the backward differential system corresponding to the characteristic curves, it is often performed through a high order splitting scheme in time, such as composition (first order for the Lie splitting, second order for the Strang splitting, or the composition of the Lie splitting with its adjoint, ...). Thus, we are going to use the Scovel splitting in combination with the composition scheme to approximate the solution $f_\varepsilon$ of the Vlasov-Poisson system (1). The solution $f_\varepsilon$ at time $t^{n+1}$ up to first order can be written as (this is well-known Lie method based on the Scovel splitting)

$$\Gamma_{\Delta t}^{\text{Lie}}[f_\varepsilon(t^n)] = f_\varepsilon(t^{n+1}) + \mathcal{O}(\Delta t^2),$$

where

$$\Gamma_{\Delta t}^{\text{Lie}}[f_\varepsilon(t^n)] = \gamma_\varepsilon^2(t^n + \Delta t) \circ \gamma_\varepsilon^1(t^n + \Delta t)[f_\varepsilon(t^n)].$$

The Strang splitting scheme based on the Scovel method (which is a second order accurate splitting method) is given by

$$\Gamma_{\Delta t}^{\text{Strang}}[f_\varepsilon(t^n)] = f_\varepsilon(t^{n+1}) + \mathcal{O}(\Delta t^3),$$

with

$$\Gamma_{\Delta t}^{\text{Strang}}[f_\varepsilon(t^n)] = \gamma_\varepsilon^1(t^n + \Delta t/2) \circ \gamma_\varepsilon^2(t^n + \Delta t) \circ \gamma_\varepsilon^1(t^n + \Delta t/2)[f_\varepsilon(t^n)]. \tag{33}$$

To achieve the second order accuracy as Strang splitting, one can consider the composition of a first-order method, such as the Lie method with its adjoint, as discussed in [4]. The composition with adjoint method based on the Scovel method is formulated as follows:

$$\begin{aligned} \Gamma_{\Delta t}^{\text{Compo}}[f_\varepsilon(t^n)] &= (\Gamma_{\Delta t/2}^{\text{Lie}})^\star \circ (\Gamma_{\Delta t/2}^{\text{Lie}})[f_\varepsilon(t^n)] \\ &= \left(\gamma_\varepsilon^2(t^n + \Delta t/2) \circ \gamma_\varepsilon^1(t^n + \Delta t/2)\right)^\star \circ \left(\gamma_\varepsilon^2(t^n + \Delta t/2) \circ \gamma_\varepsilon^1(t^n + \Delta t/2)\right)[f_\varepsilon(t^n)], \end{aligned} \tag{34}$$

where the adjoint method $(\Gamma^{\text{Lie}}_{\Delta t})^\star$ of the Lie method is the inverse map of the origin method with reserved time step, and thus it can be written as:

$$(\Gamma^{\text{Lie}}_{\Delta t/2})^\star = (\Gamma^{\text{Lie}}_{-\Delta t/2})^{-1} = (\gamma^1_\varepsilon(t^n - \Delta t/2))^{-1} \circ (\gamma^2_\varepsilon(t^n - \Delta t/2))^{-1}.$$

It is easily seen from (24) that $(\gamma^2_\varepsilon(t^n - \Delta t/2))^{-1} = \gamma^2_\varepsilon(t^n + \Delta t/2)$. We consider now the adjoint solution of $\gamma^1_\varepsilon(t^n + \Delta t)$, which is $(\gamma^1_\varepsilon(t^n - \Delta t))^{-1}$. Thanks to (25), it can be expressed as:

$$\big(\gamma^1_\varepsilon(t^n + \Delta t)\big)^\star = \big(\gamma^1_\varepsilon(t^n - \Delta t)\big)^{-1} = f_\varepsilon(t^n, X_\varepsilon(t^n - \Delta t; t^n), V_\varepsilon(t^n - \Delta t; t^n)).$$

Thus, from (23), we have $(X_\varepsilon, V_\varepsilon)(t^n - \Delta t; t^n) = (X_\varepsilon, V_\varepsilon)(t^n; t^n + \Delta t)$, implying that $\big(\gamma^1_\varepsilon(t^n + \Delta t)\big)^\star = \gamma^1_\varepsilon(t^n + \Delta t)$. Consequently, $\big(\gamma^1_\varepsilon(t^n + \Delta t)\big)^\star$ remains an exact solution of equation (5). Therefore, we can use the decomposition as in (26) to compute the adjoint solution. For symmetric composition with the adjoint method, the matrix created by $\binom{X_\varepsilon(t^n - \Delta t; t^n)}{V_\varepsilon(t^n - \Delta t; t^n)}$ can be decomposed into two shears that are the inverse of the product of two matrices in (26) with the time step reversed

$$\begin{pmatrix} 1 & 0 & \frac{\varepsilon}{\omega_c}\sin(-\theta) & \frac{\varepsilon}{\omega_c}(\cos(\theta) - 1) \\ 0 & 1 & \frac{\varepsilon}{\omega_c}(1 - \cos(\theta)) & \frac{\varepsilon}{\omega_c}\sin(-\theta) \\ 0 & 0 & 1 & 0 \\ 0 & 0 & 0 & 1 \end{pmatrix} \begin{pmatrix} 1 & 0 & 0 & 0 \\ 0 & 1 & 0 & 0 \\ 0 & 0 & \cos(\theta) & \sin(-\theta) \\ 0 & 0 & \sin(\theta) & \cos(\theta) \end{pmatrix}, \ \theta = \frac{\omega_c}{\varepsilon^2}\Delta t, \qquad (35)$$

where the second matrix is decomposed into three shears as (31) and the first matrix can be into a product of four shear transformations:

$$\begin{pmatrix} 1 & 0 & 0 & 0 \\ 0 & 1 & 0 & \frac{\varepsilon}{\omega_c}\sin(-\theta) \\ 0 & 0 & 1 & 0 \\ 0 & 0 & 0 & 1 \end{pmatrix} \begin{pmatrix} 1 & 0 & 0 & \frac{\varepsilon}{\omega_c}(\cos(\theta) - 1) \\ 0 & 1 & 0 & 0 \\ 0 & 0 & 1 & 0 \\ 0 & 0 & 0 & 1 \end{pmatrix} \begin{pmatrix} 1 & 0 & 0 & 0 \\ 0 & 1 & \frac{\varepsilon}{\omega_c}(1 - \cos(\theta)) & 0 \\ 0 & 0 & 1 & 0 \\ 0 & 0 & 0 & 1 \end{pmatrix} \begin{pmatrix} 1 & 0 & \frac{\varepsilon}{\omega_c}\sin(-\theta) & 0 \\ 0 & 1 & 0 & 0 \\ 0 & 0 & 1 & 0 \\ 0 & 0 & 0 & 1 \end{pmatrix}.$$

Finally, since $\big(\gamma^2_\varepsilon(t^n + \Delta t/2)\big)^\star = \gamma^2_\varepsilon(t^n + \Delta t/2)$ and $\big(\gamma^1_\varepsilon(t^n + \Delta t/2)\big)^\star = \gamma^1_\varepsilon(t^n + \Delta t/2)$ we obtain

$$\begin{aligned} \Gamma^{\text{Compo}}_{\Delta t} &= \big(\gamma^1_\varepsilon(t^n + \Delta t/2)\big)^\star \circ \big(\gamma^2_\varepsilon(t^n + \Delta t/2)\big)^\star \circ \gamma^2_\varepsilon(t^n + \Delta t/2) \circ \gamma^1_\varepsilon(t^n + \Delta t/2) \\ &= \gamma^1_\varepsilon(t^n + \Delta t/2) \circ \gamma^2_\varepsilon(t^n + \Delta t/2) \circ \gamma^2_\varepsilon(t^n + \Delta t/2) \circ \gamma^1_\varepsilon(t^n + \Delta t/2) = \Gamma^{\text{Strang}}_{\Delta t}. \end{aligned}$$

Therefore the composed Scovel coincides with the Strang splitting based on the Scovel method and so it is of order 2 in time.

### 3.2 Numerical scheme

This section is dedicated to constructing a second-order numerical scheme in time for the Scovel splitting (5)-(6) using the semi-Lagrangian method introduced in subsection 3.1. To simplify the presentation, we will first analyze the first-order numerical scheme, formally verifying that this scheme can provide a consistent discretization of the guiding center approximation under certain conditions

Assume that the initial distribution $f_0 \in C^1_c(\mathbb{R}^2 \times \mathbb{R}^2)$ whose support is included in some $\Omega = [-R, R]^2 \times [-v_{\max}, v_{\max}]^2 \subset \mathbb{R}^2 \times \mathbb{R}^2$ for $R > 0$, $v_{\max} > 0$ large enough. We introduce the finite uniform mesh points $(x_{i,j}, v_{k,l})$ whose coordinates are denoted by

$$x_{i,j} = (x_i, x_j), \ (i,j) \in 0, 1, 2, ..., N_x - 1 \ \text{ and } \ v_{k,l} = (v_k, v_l), \ (k,l) \in 0, 1, 2, ..., N_v - 1,$$

to discreteze the phase-space computional domain $(x, v) \in \Omega$ where $\Delta x_1, \Delta x_2$ are the sizes of one cell in $x_i$, $x_j$ directions and $\Delta v_1, \Delta v_2$ are the sizes of one cell in $v_k, v_l$ directions.

Let $\Delta t > 0$ be the time step and denote $t^n = n\Delta t$ for $n \geq 0$ as the discretization of the $t$-variables. Then denoting $\gamma_\varepsilon^{i,n}$ with the approximation of $\gamma_\varepsilon^i(t^n,\cdot,\cdot)$, $i = 1, 2$, $f_\varepsilon^n$ with the aproximation of $f_\varepsilon(t^n,\cdot,\cdot)$ , $\rho_\varepsilon^n$ with the approximation of $\rho_\varepsilon(t^n,\cdot)$ and $E_\varepsilon^n$ with the approximation of $E_\varepsilon(t^n,\cdot)$ on the uniform mesh $(x_{i,j}, v_{k,l})_{i,j,k,l}$. Assume that the value of function $f_\varepsilon$ at the mesh points $(x_{i,j}, v_{k,l})$ at any given time $t^n$.

**The second order numerical scheme.** We apply the numerical scheme (33) or (34) which enables us to transition from time $t^n$ to $t^{n+1}$ and compute $f_\varepsilon^{n+1}(x_{i,j}, v_{k,l})$ using the characteristics backward in time. The process can be described as follows:

**(A1)** Compute the distribution function at the intermediate time $t^{n\star\star}$ between $t^{n+1/2}$ and $t^{n+1}$ at the foot of the characteristic subflow $\mathcal{E}_\varepsilon^1$, starting at $(x_{i,j}, v_{k,l})$ at time $t^{n+1}$ using the Lagrange interpolation operator. This operation is presented by the operator $\mathcal{T}_1$ as follows:

$$\mathcal{T}_1[f_\varepsilon^n](x_{i,j}, v_{k,l}) = \Pi\gamma_\varepsilon^{1,n\star\star}(x_{i,j}, v_{k,l}),$$

where

$$\gamma_\varepsilon^{1,n\star\star}(x_{i,j}, v_{k,l}) = f_\varepsilon^n(X_\varepsilon(t^{n\star\star}; t^{n+1}, x_{i,j}, v_{k,l}), V_\varepsilon(t^{n\star\star}; t^{n+1}, x_{i,j}, v_{k,l})),$$

with

$$\begin{cases} X_\varepsilon(t^{n\star\star}; t^{n+1}, x_{i,j}, v_{k,l}) = x_{i,j} + \left[\mathcal{R}\left(\dfrac{\omega_c}{\varepsilon^2}\dfrac{\Delta t}{2} + \pi/2\right) - \mathcal{R}(\pi/2)\right]\varepsilon\dfrac{v_{k,l}}{\omega_c}, \\ V_\varepsilon(t^{n\star\star}; t^{n+1}, x_{i,j}, v_{k,l}) = \mathcal{R}\left(\dfrac{\omega_c}{\varepsilon^2}\dfrac{\Delta t}{2}\right)v_{k,l}. \end{cases} \tag{36}$$

Note that the interpolation used in this step follows the splitting strategy introduced in subsection 3.1. The output from above is integrated with respect to velocity to provide an approximation for the density at time $t^{n+1/2}$,

$$\rho_\varepsilon^{n+1/2}(x_{i,j}) = \int_{\mathbb{R}^2} \mathcal{T}_1[f_\varepsilon^n](x_{i,j}, v)\mathrm{d}v,$$

which is then substituted into the Poisson equation to compute the approximation of the electric field at time $t^{n+1/2}$, that is

$$E_{\varepsilon,i,j}^{n+1/2} := E_\varepsilon^{n+1/2}(x_{i,j}) = -\nabla_x\Phi_\varepsilon^{n+1/2}(x_{i,j}), \quad -\epsilon_0\Delta_x\Phi_\varepsilon^{n+1/2}(x_{i,j}) = q\int_{\mathbb{R}^2}\mathcal{T}_1[f_\varepsilon^n](x_{i,j}, v)\mathrm{d}v.$$

**(A2)** The result obtained from **(A1)** computes the distribution function at time $t^{n+1/2}$ at the foot of the characteristic subflow $\mathcal{E}_\varepsilon^2$, starting at $(x_{i,j}, v_{k,l})$ at time $t^{n\star\star}$ with the electric field $E_{\varepsilon,i,j}^{n+1/2}$ using the Lagrange interpolation operator. This action is described by the operator $\mathcal{T}_2$ as follows:

$$\mathcal{T}_2[f_\varepsilon^n](x_{i,j}, v_{k,l}) = \Pi\gamma_\varepsilon^{2,n+1/2}(x_{i,j}, v_{k,l}),$$

where

$$\gamma_\varepsilon^{2,n+1/2}(x_{i,j}, v_{k,l}) = f_\varepsilon^n(X_\varepsilon(t^{n+1/2}; t^{n\star\star}, x_{i,j}, v_{k,l}), V_\varepsilon(t^{n+1/2}; t^{n\star\star}, x_{i,j}, v_{k,l})),$$

with

$$\begin{cases} X_\varepsilon(t^{n+1/2}; t^{n\star\star}, x_{i,j}, v_{k,l}) = x_{i,j}, \\ V_\varepsilon(t^{n+1/2}; t^{n\star\star}, x_{i,j}, v_{k,l}) = v_{k,l} - \dfrac{q}{m}\dfrac{\Delta t}{2\varepsilon}E_{\varepsilon,i,j}^{n+1/2}. \end{cases} \tag{37}$$

**(A3)** The result obtained from **(A2)** is evaluated at intermediate time $t^{n_\star}$ between $t^n$ and $t^{n+1/2}$ at the foot of the characteristic subflow $\mathcal{E}_\varepsilon^2$, starting at $(x_{i,j}, v_{k,l})$ at time $t^{n+1/2}$ with the electric field $E_{\varepsilon,i,j}^{n+1/2}$ using the Lagrange interpolation operator. This action is written by:

$$\mathcal{T}_2[f_\varepsilon^n](x_{i,j}, v_{k,l}) = \Pi\gamma_\varepsilon^{2,n_\star}(x_{i,j}, v_{k,l}),$$

where

$$\gamma_\varepsilon^{2,n_\star}(x_{i,j}, v_{k,l}) = f_\varepsilon^n(X_\varepsilon(t^{n_\star}; t^{n+1/2}, x_{i,j}, v_{k,l}), V_\varepsilon(t^{n_\star}; t^{n+1/2}, x_{i,j}, v_{k,l})),$$

with the characteristic curves $X_\varepsilon(t^{n_\star}; t^{n+1/2}, x_{i,j}, v_{k,l})$ and $V_\varepsilon(t^{n_\star}; t^{n+1/2}, x_{i,j}, v_{k,l})$ are defined as in the right hand side of (37).

**(A4)** The result obtained from **(A3)** is computed at time $t^n$ at the foot of the characteristic subflow $\mathcal{E}_\varepsilon^1$ starting at $(x_{i,j}, v_{k,l})$ at time $t^{n_\star}$ using the Lagrange interpolation operator. This action is described by

$$\mathcal{T}_1[f_\varepsilon^n](x_{i,j}, v_{k,l}) = \Pi\gamma_\varepsilon^{1,n}(x_{i,j}, v_{k,l}),$$

where

$$\gamma_\varepsilon^{1,n}(x_{i,j}, v_{k,l}) = f_\varepsilon^n(X_\varepsilon(t^n; t^{n_\star}, x_{i,j}, v_{k,l}), X_\varepsilon(t^n; t^{n_\star}, x_{i,j}, v_{k,l})),$$

with the characteristic curves $X_\varepsilon(t^n; t^{n_\star}, x_{i,j}, v_{k,l})$ and $V_\varepsilon(t^n; t^{n_\star}, x_{i,j}, v_{k,l})$ are defined as in (36) on the time step $\Delta t/2$.

Finally, the second order numerical scheme is written by

$$f_\varepsilon^{n+1}(x_{i,j}, v_{k,l}) = \mathcal{T}_1 \circ \mathcal{T}_2 \circ \mathcal{T}_2 \circ \mathcal{T}_1[f_\varepsilon^n](x_{i,j}, v_{k,l}), \tag{38}$$

and we then compute the particle density $\rho_\varepsilon^{n+1}$ given by

$$\rho_\varepsilon^{n+1}(x_{i,j}) = \Delta v_1 \Delta v_2 \sum_{k,l=0}^{N_v-1} f_\varepsilon^{n+1}(x_{i,j}, v_{k,l}). \tag{39}$$

**Remark 3.3** *If we use such a method, due to the $\frac{1}{\varepsilon}$-frequency oscillations of the electric field in* (37)*, we have to guarantee the accurate simulation of the scheme using the semi-Lagrangian solver. Therefore, the time step $\Delta t$ must satisfy the following condition:*

$$\Delta t < \mathcal{O}(\varepsilon v_{max}), \tag{40}$$

*where $v_{max}$ is denoted as the maximum value in the velocity grid.*

**The asymptotic limit of full discretization for density by formal arguments.** We now aim to formally investigate the asymptotic limit property of the fully discretized density $\rho_\varepsilon^{n+1}(x_{i,j})$ in (39), as $\varepsilon \to 0$. For simplicity, we will focus on the first order in time numerical scheme. In this case, the full discretized numerical scheme for the distribution function $f_\varepsilon^{n+1}$ in (38) can be expressed as:

$$f_\varepsilon^{n+1}(x_{i,j}, v_{k,l}) = \mathcal{T}_2 \circ \mathcal{T}_1[f_\varepsilon^n](x_{i,j}, v_{k,l}), \tag{41}$$

where the operators $\mathcal{T}_i$, $i = 1, 2$ are given in steps **(Ai)** respectively on the time step $\Delta t$. We then compute the particle density $\rho_\varepsilon^{n+1}$ given by

$$\rho_\varepsilon^{n+1}(x_{i,j}) = \Delta v_1 \Delta v_2 \sum_{k,l=0}^{N_v-1} f_\varepsilon^{n+1}(x_{i,j}, v_{k,l}). \tag{42}$$

Before passing to the limit, we need the following lemma:

**Lemma 3.1** *Let us consider a time step $\Delta t > 0$, a final time $T > 0$ and set $N_T = [T/\Delta t]$. Assuming that the initial distribution function $f_0(x, v)$ whose support is included in $\Omega = [-R, R]^2 \times [-v_{max}, v_{max}]^2$ and $(f_\varepsilon^{n+1})_{0\le n\le N_T-1}$ is the numerical solution of the Vlasov-Poisson system, computed by the numerical scheme in (41). Then, for $0 \le n \le N_T - 1$, we have*

$$\gamma_\varepsilon^{1,n+1}(x_{i,j}, v_{k,l}) = \gamma_\varepsilon^{1,n+1}(x_{i,j} - \varepsilon\frac{^\perp v_{k,l}}{\omega_c}, v_{k,l}) + \mathcal{O}(\varepsilon). \tag{43}$$

*Consequently, we get*

$$\begin{aligned}&\gamma_\varepsilon^{2,n+1} \circ \gamma_\varepsilon^{1,n+1}(x_{i,j}, v_{k,l})\\ &= f_\varepsilon^n(x_{i,j} + \mathcal{R}\left(\frac{\omega_c}{\varepsilon^2}\Delta t + \frac{\pi}{2}\right)\varepsilon\frac{v_{k,l}}{\omega_c}, \mathcal{R}\left(\frac{\omega_c}{\varepsilon^2}\Delta t\right) v_{k,l} - \frac{q}{m}\frac{\Delta t}{\varepsilon}E_{\varepsilon,i,j}^{n+1}) + \mathcal{O}(\varepsilon).\end{aligned}$$

**Proof.** Since

$$\begin{aligned}\gamma_\varepsilon^{1,n+1}(x_{i,j}, v_{k,l}) &= f_\varepsilon^n(X_\varepsilon(t^{n+1/2}; t^{n+1}, x_{i,j}, v_{k,l}), V_\varepsilon(t^{n+1/2}; t^{n+1}, x_{i,j}, v_{k,l}))\\ &= f_\varepsilon^n(x_{i,j} + \left[\mathcal{R}\left(\frac{\omega_c}{\varepsilon^2}\Delta t + \frac{\pi}{2}\right) - \mathcal{R}\left(\frac{\pi}{2}\right)\right]\varepsilon\frac{v_{k,l}}{\omega_c}, \mathcal{R}\left(\frac{\omega_c}{\varepsilon^2}\Delta t\right) v_{k,l}),\end{aligned}$$

we get

$$\begin{aligned}&\gamma_\varepsilon^{1,n+1}(x_{i,j} - \varepsilon\frac{^\perp v_{k,l}}{\omega_c}, v_{k,l})\\ &\quad= f_\varepsilon^n(x_{i,j} - \varepsilon\frac{^\perp v_{k,l}}{\omega_c} + \left[\mathcal{R}\left(\frac{\omega_c}{\varepsilon^2}\Delta t + \frac{\pi}{2}\right) - \mathcal{R}\left(\frac{\pi}{2}\right)\right]\varepsilon\frac{v_{k,l}}{\omega_c}, \mathcal{R}\left(\frac{\omega_c}{\varepsilon^2}\Delta t\right) v_{k,l})\\ &\quad= f_\varepsilon^n(x_{i,j} + \mathcal{R}\left(\frac{\omega_c}{\varepsilon^2}\Delta t + \frac{\pi}{2}\right)\varepsilon\frac{v_{k,l}}{\omega_c}, \mathcal{R}\left(\frac{\omega_c}{\varepsilon^2}\Delta t\right) v_{k,l}).\end{aligned}$$

Hence we deduce by the mean-value theorem that

$$|\gamma_\varepsilon^{1,n+1}(x_{i,j}, v_{k,l}) - \gamma_\varepsilon^{1,n+1}(x_{i,j} - \varepsilon\frac{^\perp v_{k,l}}{\omega_c}, v_{k,l})| \le \frac{\varepsilon}{\omega_c}\|\nabla f_\varepsilon^n\|_\infty |v_{k,l}| \le C\varepsilon,$$

where $C = C(\omega_c, \|f_0\|_{W^{1,\infty}}, v_{\max})$ and thus it implies (43). Finally, we act $\gamma_\varepsilon^{2,n+1}$ to both side of (43) noting that

$$\begin{aligned}\gamma_\varepsilon^{2,n+1}(x_{i,j}, v_{k,l}) &= f_\varepsilon^n(X_\varepsilon(t^n; t^{n+1/2}, x_{i,j}, v_{k,l}), V_\varepsilon(t^n; t^{n+1/2}, x_{i,j}, v_{k,l}))\\ &= f_\varepsilon^n(x_{i,j}, v_{k,l} - \frac{q}{m}\frac{\Delta t}{\varepsilon}E_{\varepsilon,i,j}^{n+1}),\end{aligned}$$

and thus we obtain

$$\begin{aligned}\gamma_\varepsilon^{2,n+1} \circ \gamma_\varepsilon^{1,n+1}(x_{i,j}, v_{k,l}) &= \gamma_\varepsilon^{2,n+1} \circ \left[\gamma_\varepsilon^{1,n+1}(x_{i,j} - \varepsilon\frac{^\perp v_{k,l}}{\omega_c}, v_{k,l})\right] + \mathcal{O}(\varepsilon)\\ &= f_\varepsilon^n(x_{i,j} + \mathcal{R}\left(\frac{\omega_c}{\varepsilon^2}\Delta t + \frac{\pi}{2}\right)\varepsilon\frac{v_{k,l}}{\omega_c}, \mathcal{R}\left(\frac{\omega_c}{\varepsilon^2}\Delta t\right) v_{k,l} - \frac{q}{m}\frac{\Delta t}{\varepsilon}E_{\varepsilon,i,j}^{n+1}) + \mathcal{O}(\varepsilon),\end{aligned}$$

which implies the desired result. □

**Proposition 3.1** ***(Formal)**. Assuming that the initial distribution function $f_0(x, v)$ whose support is included in $\Omega = [-R, R]^2 \times [-v_{max}, v_{max}]^2$. Let us consider a time step $\Delta t > 0$ satisfied the condition (40), a final time $T > 0$ and set $N_T = [T/\Delta t]$. Assume that the sequence $(\rho_\varepsilon^{n+1})_{0\le n\le N_T-1}$ is given by (42). Then, for $0 \le n \le N_T - 1$, $\rho_\varepsilon^{n+1} \to \rho^{n+1}$, as $\varepsilon \to 0$ and the limit $(\rho^{n+1})_{0\le n\le N_T-1}$ is a consistent first order approximation with respect to $\Delta t$ of the guiding center equation provided by the semi-Lagrangian method*

$$\rho^{n+1}(x_{i,j}) \approx \Pi\rho^n(x_{i,j} - \Delta t\frac{^\perp E_{i,j}^{n+1}}{B}). \tag{44}$$

**Proof.** First, we rewrite the formula of the distribution function $f_\varepsilon^{n+1}$ in (41) as:

$$\mathcal{T}_2 \circ \mathcal{T}_1[f_\varepsilon^n](x_{i,j}, v_{k,l}) = \Pi[\gamma_\varepsilon^{2,n+1} \circ \gamma_\varepsilon^{1,n+1}](x_{i,j}, v_{k,l}) + \mathcal{O}((\Delta x_1)^p(\Delta x_2)^p) + \mathcal{O}((\Delta v_1)^p(\Delta v_2)^p),$$

where $p$ denotes the degree of the Lagrange interpolation operator. Therefore, by taking into account the fine phase space mesh, we can anticipate that

$$\mathcal{T}_2 \circ \mathcal{T}_1[f_\varepsilon^n](x_{i,j}, v_{k,l}) \approx \Pi[\gamma_\varepsilon^{2,n+1} \circ \gamma_\varepsilon^{1,n+1}](x_{i,j}, v_{k,l}),$$

where $[\gamma_\varepsilon^{2,n+1} \circ \gamma_\varepsilon^{1,n+1}](x_{i,j}, v_{k,l}) = f_\varepsilon^n(X_\varepsilon(t^n; t^{n+1}, x_{i,j}, v_{k,l}), V_\varepsilon(t^n; t^{n+1}, x_{i,j}, v_{k,l}))$ with

$$\begin{cases} X_\varepsilon(t^n; t^{n+1}, x_{i,j}, v_{k,l}) = x_{i,j} + \left[\mathcal{R}\left(\dfrac{\omega_c}{\varepsilon^2}\Delta t + \pi/2\right) - \mathcal{R}(\pi/2)\right] \varepsilon \dfrac{v_{k,l}}{\omega_c}, \\ V_\varepsilon(t^n; t^{n+1}, x_{i,j}, v_{k,l}) = \mathcal{R}\left(\dfrac{\omega_c}{\varepsilon^2}\Delta t\right) v_{k,l} - \dfrac{q}{m}\dfrac{\Delta t}{\varepsilon} E_{\varepsilon,i,j}^{n+1}. \end{cases}$$

Next, provide a formal proof demonstrating that the particle density $\rho_\varepsilon^{n+1}$ obtained from $f_\varepsilon^n$ as

$$\rho_\varepsilon^{n+1}(x_{i,j}) \approx \Delta v_1 \Delta v_2 \sum_{k,l=0}^{N_v-1} \Pi f_\varepsilon^n(X_\varepsilon(t^n; t^{n+1}, x_{i,j}, v_{k,l}), V_\varepsilon(t^n; t^{n+1}, x_{i,j}, v_{k,l})) \tag{45}$$

is a consistent first order approximation with respect to $\Delta t$ of the guiding center model. That means

$$\rho_\varepsilon^n \to \rho^n, \quad \text{as } \varepsilon \to 0,$$

and the limit $(\rho^n)_n$ is a first order numerical solution with respect to $\Delta t$ of the guiding center equation provided by the backward semi-Lagrangian method. Indeed, thanks to Lemma 3.1, we deduce

$$\begin{aligned} &\Delta v_1 \Delta v_2 \sum_{k,l=0}^{N_v-1} \Pi[\gamma_\varepsilon^{2,n+1} \circ \gamma_\varepsilon^{1,n+1}](x_{i,j}, v_{k,l}) \\ &= \Delta v_1 \Delta v_2 \sum_{k,l=0}^{N_v-1} \Pi f_\varepsilon^n(x_{i,j} - \varepsilon \mathcal{R}\left(\frac{\omega_c}{\varepsilon^2}\Delta t\right) \frac{^\perp v_{k,l}}{\omega_c}, \mathcal{R}\left(\frac{\omega_c}{\varepsilon^2}\Delta t\right) v_{k,l} - \frac{q}{m}\frac{\Delta t}{\varepsilon} E_{\varepsilon,i,j}^{n+1}) + \mathcal{O}(\varepsilon) \\ &= \Delta v_1 \Delta v_2 \sum_{k,l=0}^{N_v-1} \Pi f_\varepsilon^n(x_{i,j} - \varepsilon \frac{^\perp v_{k,l}}{\omega_c}, v_{k,l} - \frac{q}{m}\frac{\Delta t}{\varepsilon} E_{\varepsilon,i,j}^{n+1}) + \mathcal{O}(\Delta v_1 \Delta v_2) + \mathcal{O}(\varepsilon), \end{aligned}$$

where we used the change of variable $v_{k,l} \mapsto \mathcal{R}(-\frac{\omega_c}{\varepsilon^2}\Delta t) v_{k,l}$ to filter the fast rotation in velocity. The error $\mathcal{O}(\Delta v_1 \Delta v_2)$ arises from the discrete integral over the velocity variable not being conserved by a rotation. Subsequently, we perform the translation $v_{k,l} \mapsto v_{k,l} + \frac{q}{m}\frac{\Delta t}{\varepsilon} E_{\varepsilon,i,j}^{n+1}$ to eliminate the stiff term, with the condition (40) to ensure that this change of variable is well defined in the velocity grid. Therefore, if we consider a fine mesh in the direction of velocity, we can expect that the particle density $\rho_\varepsilon^{n+1}$ in (45) can be approximated by

$$\rho_\varepsilon^{n+1}(x_{i,j}) \approx \Delta v_1 \Delta v_2 \sum_{k,l=0}^{N_v-1} \Pi f_\varepsilon^n(x_{i,j} - \Delta t \frac{^\perp E_{\varepsilon,i,j}^{n+1}}{B} - \varepsilon \frac{^\perp v_{k,l}}{\omega_c}, v_{k,l}) + \mathcal{O}(\varepsilon). \tag{46}$$

Formally passing to the limit as $\varepsilon \to 0$ in (46), we obtain that

$$\begin{aligned} \rho^{n+1}(x_{i,j}) &\approx \Delta v_1 \Delta v_2 \sum_{k,l=0}^{N_v-1} \Pi f^n(x_{i,j} - \Delta t \frac{^\perp E_{i,j}^{n+1}}{B}, v_{k,l}) \\ &= \Pi \rho^n(x_{i,j} - \Delta t \frac{^\perp E_{i,j}^{n+1}}{B}), \end{aligned}$$

which is a consistent first order approximation with respect to $\Delta t$ of the guiding center model provided by the semi-Lagrangian method. □

**Remark 3.4** *In a manner similar to the proof for the second order in time numerical scheme, we can conclude that the limit of particle density* $\rho_\varepsilon^{n+1}(x_{i,j})$ *given by* (39) *approximates to* $\rho^{n+1}(x_{i,j})$ *as* $\varepsilon$ *goes to zero satisfying the following equation*

$$\rho^{n+1}(x_{i,j}) \approx \Pi\rho^n(x_{i,j} - \Delta t\frac{^\perp E_{i,j}^{n+1/2}}{B}),$$

*which is a consistent second-order approximation with respect to* $\Delta t$ *of the guiding center model provided by the semi-Lagrangian method.*

# 4 Numerical Simulation

In this section, we present numerical results obtained using various time discretization schemes described in Sections 2 and 3 for solving the Vlasov-Poisson system (1). Comparisons between methods will be conducted over a wide range of $\varepsilon$ to illustrate their capabilities and limitations. We consider the Vlasov-Poisson system (1) with the Kelvin-Helmholtz instability type initial data

$$f_0(x,v) = (1 + \sin(k_2x_2) + \nu\cos(k_1x_1))\frac{1}{2\pi}\exp\left(-\frac{{v_1}^2 + {v_2}^2}{2}\right), \tag{47}$$

defined in $\Omega_x \times \Omega_v$, where $\Omega_x = [0, L_1] \times [0, L_2]$ is the periodic domain with the lengths $L_d = 2\pi/k_d$, $d = 1, 2$, $k_d = (k_1, k_2) = (0.4, 1)$, the amplitude $\nu = 0.015$ and $\Omega_v = [-v_{\max}, v_{\max}]^2$, $v_{\max} = 8$. Then the initial density of the guiding center approximation (2) is expressed as:

$$\rho_0(x) = 1 + \sin(k_2x_2) + \nu\cos(k_1x_1), \tag{48}$$

defined in $\Omega_x$. The numerical parameters are $N_x$ points in space, $N_v$ points per velocity direction.

We perform simulations using the BSL method for the Vlasov-Poisson equation (1) on the phase space grid. Initially,we investigate the second order explicit scheme in time (16)-(17). Subsequently, we implement second-order time-accurate methods, including the composition method (Strang method or composition with adjoint), coupled with the splitting technique (Scovel splitting, exponential Boris algorithm). On the other hand, we compute an approximation of the guiding center model (2) using a backward semi-Lagrangian method developed in [19] with Lagrange interpolation. This reference will be used to compare our results obtained from the Vlasov-Poisson system with a large magnetic field for a long time.

First of all, we are interested in the time evolution of the electrostatic energy in the first dimension $\frac{1}{2}\|E_1\|_2^2$ for several $\varepsilon$.

**4D case:**

In Figure 1, we first investigate numerically the convergence of the Vlasov-Poisson system (1) toward its limit model (2). We set the numerical parameters as follows: $\Delta t = 0.1$, $N_x = 128$, $N_v = 32$ and consider different values of $\varepsilon$ ranging from $10^{-4}$ to 1. We observe that the Vlasov-Poisson solution does not approach the guiding center solution closely when $\varepsilon = 0.1, 1$. However, for smaller values of $\varepsilon$, these results confirm the strong convergence of the Vlasov-Poisson equation (1) towards the asymptotic model (2). Simulations for $\varepsilon = 10^{-3}$ and $10^{-4}$ display a qualitatively very good match between the Vlasov-Poisson reference solution and the guiding center solution. Then, proceeding further, we will perform numerical experiments to yield accurate long-time simulations long time simulations of this method under varying $\Delta t$ and $N_x$. The error behavior with respect to time for different discretizations in space can be written cf. [7]

$$\mathcal{O}(\Delta t^2) + \mathcal{O}((\max(\Delta x_1, \Delta x_2)^{p+1}/\Delta t) + \mathcal{O}(\max(\Delta v_1, \Delta v_2)^{p+1}/\Delta t).$$

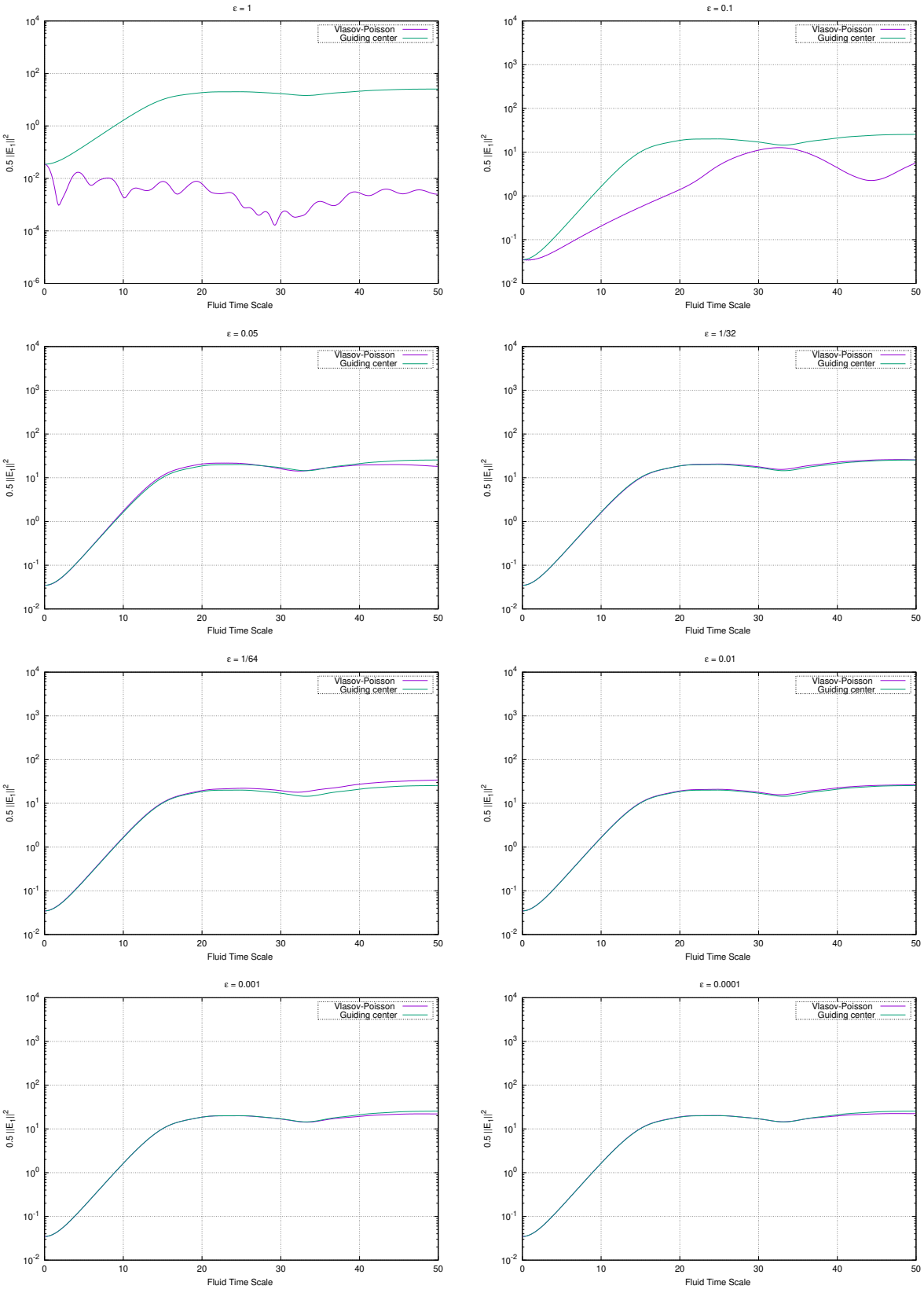


Figure 1: Time evolution of $0.5\|E_\varepsilon^1\|_2^2$ for the Vlasov-Poisson model for final time $T = 50$, $N_x = 128$, $N_v = 32$, and $\Delta t = 0.1$.

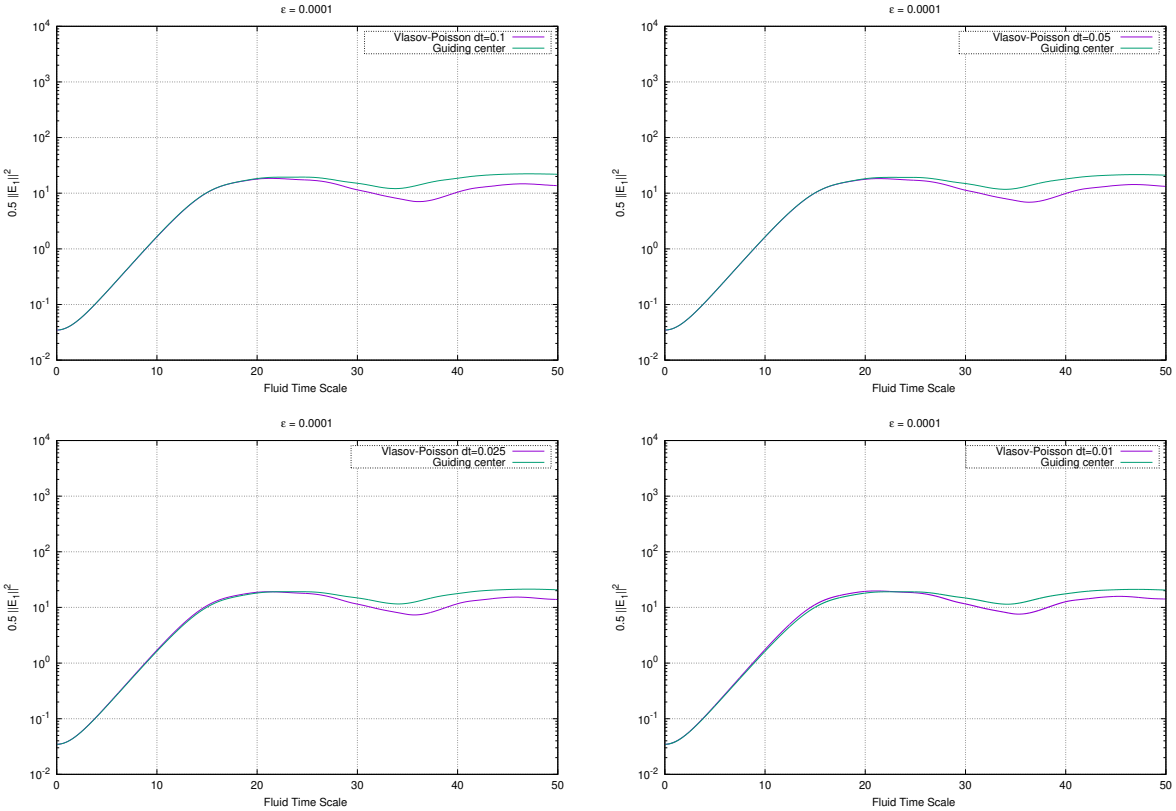


Figure 2: Time evolution of electrostatic energy in the first dimension for the Vlasov-Poisson model with $N_x = 32$, $N_v = 32$. From left to right we present the $\frac{1}{2}\|E_1\|_2^2$ at $\Delta t = 0.1$, $\Delta t = 0.05$, $\Delta t = 0.025$, and $\Delta t = 0.01$.

In Figure 2, we explore various time step values: $\Delta t \in \{0.1, 0.05, 0.025, 0.01\}$ for a fixed coarse mesh with $N_x = 32, N_v = 32$ to observe the influence of the time step. As $\Delta t$ decreases from 0.1 to 0.05, we observe similar behavior in the plots. However, for smaller time steps, the results are less accurate. This discrepancy arises because we use Lagrangian interpolation with a coarse mesh, which performs poorly when the time step is small. In Figure 3, we fix the time step $\Delta t = 0.1$. To assess the impact of the number of points in the grid, we vary $N_x$ from the set $\{32, 64, 128\}$ while keeping $N_v = 32$ constant. We observe that the solution on the coarse grid is less accurate over the long term compared to the solution on the finer grid, primarily due to spatial errors. In conclusion, to obtain sufficiently accurate solutions in long-time simulations, the time step should not be too small, and the mesh should not be too coarse. Finally, in Figure 4, we compare the result between the second order BSL method (16)-(17) and those of Remark 2.4 after filtering the rotation. The results show that the two methods exhibit the same performance.

**Splitting case:**

Firstly, our focus is on comparing various methods in the intermediate regime of $\varepsilon$: the Strang splitting based on the exponential Boris algorithm, the Strang splitting, and the composition with the adjoint of Scovel's method. This comparison is conducted across a range from weak to strong magnetic fields while maintaining a constant number of time steps. In Figure 5, we plot the time evolution of the electrostatic energy in the first dimension with different values of $\varepsilon$, ranging from 1 to 1/132. We compare the numerical results obtained with these schemes to a numerical solution for the guiding center model. The simulation runs up to a final time $T = 50$ with a fixed time step $\Delta t = 0.01$. For $\varepsilon = 1, 1/2, 1/4$, and $1/8$,

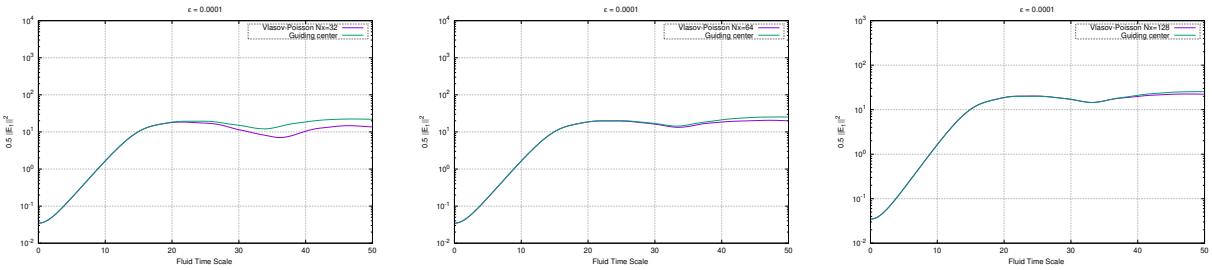


Figure 3: Time evolution of electrostatic energy in the first dimension for the Vlasov-Poisson model. From left to right we present the $\frac{1}{2}\|E_1\|_2^2$ at $N_x = 32$, $N_x = 64$, and $N_x = 128$.

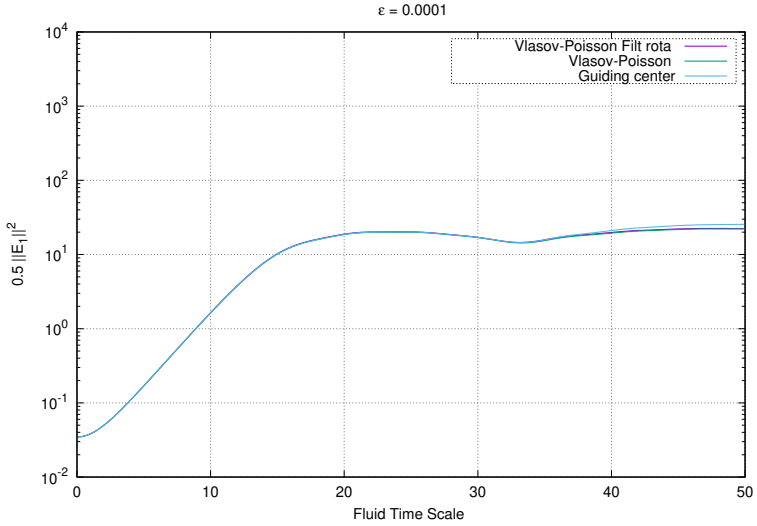


Figure 4: Time evolution of electrostatic energy in the first dimension for the Vlasov-Poisson model for final time $T = 50$, $\Delta t = 0.1$, and $N_x = 128$, $N_v = 32$.

all integrators exhibit similar performance. However, as $\varepsilon$ decreases, the Scovel method is clearly better. Specifically, for $\varepsilon = 1/16, 1/32, 1/64$, and $1/132$ the Strang splitting based on the exponential Boris algorithm fails entirely due to the condition (32) not being satisfied. In contrast, the Strang splitting and the composition with adjoint based on Scovel's method remain unaffected, confirming the convergence of Vlasov-Poisson system (1) towards the asymptotic model (2) in the intermediate regime of $\varepsilon$.
Moving on to the limit regime of $\varepsilon$, we conduct a numerical investigation into the impact of condition (40) to the convergence of the Vlasov-Poisson system (1) towards its limit model (2). In Figure 6, we illustrate the time evolution of the electrostatic energy in the first dimension for different values $\varepsilon$ while maintaining fixed numerical parameters: $\Delta t = 0.01, N_x = 128$, and the ratio $N_v/v_{\max} = 4$, denoting the number of points per cell in the velocity grid. As observed in Figure 6, as the parameter $\varepsilon$ decreases, it becomes necessary to choose a larger value for $v_{\max}$ to obtain satisfactory results results. For instance, with $\varepsilon = 1/132$, we set $v_{\max} = 8$ to achieve a good simulation. However, for $\varepsilon = 1/400$ and $1/1000$, this value of $v_{\max}$ is inadequate, yielding unsatisfactory results, whereas $v_{\max} = 16$ produces better outcomes. For $\varepsilon = 1/1600$, we require $v_{\max} = 32$. In Figure 7, we present the time evolution of the electrostatic energy in the first dimension for various values $\Delta t$ when $\varepsilon = 1/32$. The value of $v_{\max}$ is adjusted based on the time step $\Delta t$ to ensure that condition (40) is satisfied. The simulation demonstrates that a large time step $\Delta t$ should be avoided to achieve good results.

In the following, we shall implement numerical comparisons between the particle density $\rho_\varepsilon$ obtained from the discretized Vlasov-Poisson system and that corresponding to the discretized guiding center model. Specifically, we present contours of particle densities in physical space at various final times $T \in \{5, 10, 18, 25\}$. We observe the time evolution of the particle density for the guiding center model using Lagrangian interpolation. Concerning the densities provided by the Vlasov-Poisson system, we initially focus on the **4-D case** with $\varepsilon = 10^{-4}$. In Figure 8, we find that the density $\rho_\varepsilon$ computed from the Vlasov-Poisson equation follows the same evolution as that of the guiding center model. Next, we consider the **splitting case** where $\varepsilon = 0.01$. In this scenario, the figures in Figure 9 illustrate the development of the instability of the density, which obeyed the same evolution as the density of the guiding center model.

Finally, we present the time evolution of particle density $\rho_\varepsilon$ in $L^2$ and $L^1$ norms for the Vlasov-Poisson solution, comparing these results with the guiding center model. In Figure 10, for the **4-D case**, we observe $\|\rho_\varepsilon\|_{L^p}^p$, $p = 1, 2$ with $\varepsilon = 10^{-4}$ using the BSL method (16)-(17) and the approach outlined in Remark 2.4. We then compare the result to those of the guiding center model. The figure show that the method in Remark 2.4 performs better on the coarser mesh in the velocity grid due to the elimination of rotation. In Figures 11 and 12, for the **splitting case**, we plot these quantities with several values of $\varepsilon$ from $1/2$ to $1/132$ to observe the convergence. We also vary the number of points in the position grid $N_x \in \{32, 64, 128, 256\}$ to assess the impact of the parameter on the accuracy of the method.

# 5 Conclusion

In this paper, we have used the semi-Lagrangian method to solve the four-dimensional Vlasov-Poisson system with a strong external uniform magnetic field. We proposed two time discretization techniques: the full Vlasov solver and the split Vlasov solver.

The full Vlasov solver employs a fully explicit scheme and can accurately handle large time steps with respect to the typical size of the solution's fast oscillations. Additionally, we have shown numerically that this method provides a consistent discretization with respect to

the limiting guiding center model.

The splitting schemes for the Vlasov equation are based on the exponential Boris algorithm and the Scovel method. The exponential Boris algorithm works badly. However, the Scovel method presented here performs well independently of the strength of the magnetic field. We can choose the time step $\Delta t$ much larger than $\mathcal{O}(\varepsilon^2)$. Nevertheless, due to the high oscillation in the electric field by the Scovel method, the time step $\Delta t$ must adhere to the condition (40) within the semi-Lagrangian method. As the parameter $\varepsilon$ becomes smaller, we need to take the larger value of $v_{\max}$ and then increase the number of points in the direction of velocity to obtain satisfactory results. Since the semi-Lagrangian schemes rely on interpolation on a phase space mesh, we have to pay attention to the number of points in the velocity grid as $v_{\max}$ increases. Therefore, for an intermediate value of $\varepsilon$, the Scovel method proves to be an appropriate approach for the Vlasov-Poisson model.

## Acknowledgements

Centre de Calcul Intensif d'Aix-Marseille is acknowledged for granting access to its high performance computing resources. This work has been carried out within the framework of the EUROfusion Consortium, funded by the European Union via the Euratom Research and Training Programme (Grant Agreement No 101052200 — EUROfusion). Views and opinions expressed are however those of the author(s) only and do not necessarily reflect those of the European Union or the European Commission. Neither the European Union nor the European Commission can be held responsible for them.

## References

[1] J. Ameres. Splitting methods for fourier spectral discretizations of the strongly magnetized vlasov-poisson and the vlasov-maxwell system. arXiv:1907.05319, 2019.

[2] R. Belaouar, N. Crouseilles, P. Degond, and E. Sonnendrücker. An asymptotically stable semi-lagrangian scheme in the quasi-neutral limit. *J. Sci. Comput.*, 41:341–365, 2009.

[3] J. Bernier. Exact splitting methods for semigroups generated by inhomogeneous quadratic differential operators. *Found. Comput. Math.*, 21:1401–1439, 2021.

[4] J. Bernier, F. Casas, and N. Crouseilles. Splitting methods for rotation: application to vlasov equations. *SIAM Methods and Algorithms Sci. Comput.*, 42:666–697, 2020.

[5] J. Bernier, N. Crouseilles, and Y. Li. Exact splitting methods for kinetic and schrödinger equations. *J. Sci. Comput. 86*, 10, 2021.

[6] C.K. Birdsall and A.B. Langdon. *Plasma Physics Via Computer Simulation.* McGraw-Hill, New York, 1985.

[7] F. Charles, B. Després, and M. Mehrenberger. Enhanced convergence estimates for semi-lagrangian schemes application to the vlasov–poisson equation. *SIAM J. Num. Anal.*, 51:840–863, 2013.

[8] N. Crouseilles, L. Einkemmer, and E. Faou. Hamiltonian splitting for the vlasov–maxwell equations. *J. Comput. Physics*, 283:224–240, 2015.

[9] N. Crouseilles, M. Lemou, F. Méhats, and X. Zhao. Uniformly accurate forward semi-lagrangian methods for highly oscillatory vlasov-poisson equations. *SIAM Multi. Model. Simu.*, 15:723–744, 2017.

[10] N. Crouseilles, M. Lemou, F. Méhats, and X. Zhao. Uniformly accurate particle-in-cell method for the long time solution of the two-dimensional vlasov–poisson equation with uniform strong magnetic field. *J. Comput. Physics*, 36:172–190, 2017.

[11] N. Crouseilles, M. Mehrenberger, and E. Sonnendrücker. Conservative semi-lagrangian schemes for vlasov equations. *J. Comput. Physics*, 229:1927–1953, 2010.

[12] F. Filbet and C. Prouveur. High order time discretization for backward semi-lagrangian methods. *J. Comput. Appl. Math.*, 303:171–188, 2016.

[13] F. Filbet and L.-M. Rodrigues. Asymptotically stable particle-in-cell methods for the vlasov-poisson system with a strong external magnetic field. *SIAM J. Num. Anal.*, 54:1120–1146, 2016.

[14] E. Frenod, S. A. Hirstoaga, M. Lutz, and E. Sonnendrücker. Long time behaviour of an exponential integrator for a vlasov-poisson system with strong magnetic field. *Commun. Comput. Physics*, 18:263–296, 2015.

[15] S. Jin. Efficient asymptotic-preserving (ap) schemes for some multiscale kinetic equations. *SIAM J. Sci. Comput.*, 21:441–454, 1999.

[16] E. Miot. On the gyrokinetic limit for the two-dimensional vlasov-poisson system. *arXiv: Analysis of PDEs*, 2016.

[17] A. Mouton. Two-scale semi-lagrangian simulation of a charged particle beam in a periodic focusing channel. *Kinetic and Related Models*, 2:251–274, 2009.

[18] L. S. Raymond. Control of large velocities in the two-dimensional gyrokinetic approximation. *J. Math. Pures Appl.*, 81:379–399, 2002.

[19] E. Sonnendrücker, J. Roche, P. Bertrand, and A. Ghizzo. The semi-lagrangian method for the numerical resolution of the vlasov equation. *J. Comput. Physics*, 149:201–220, 1999.

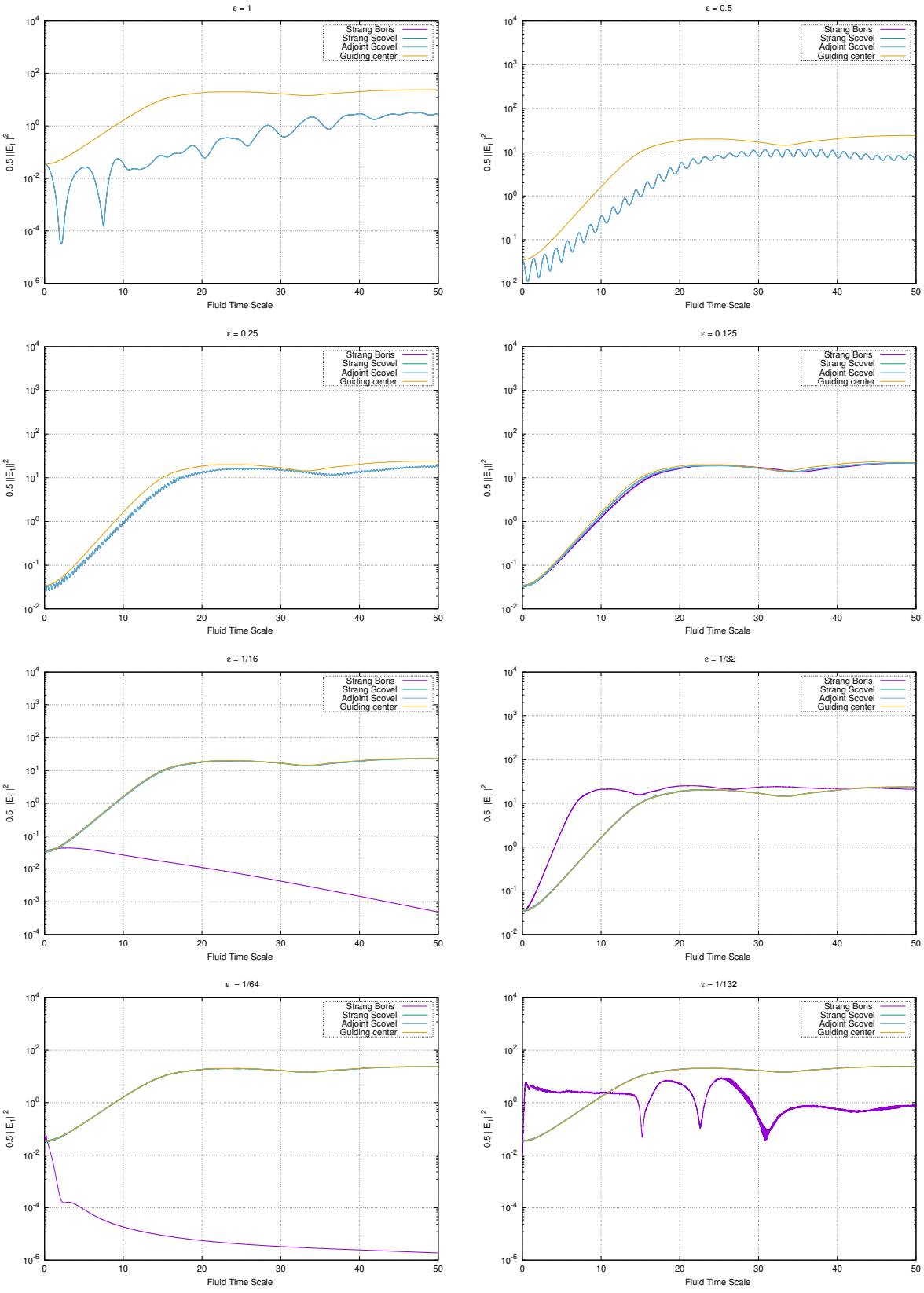


Figure 5: Comparison between the time evolution of $0.5\|E_\varepsilon^1\|_2^2$ for the Vlasov-Poisson system and the guiding center model. $N_x = 128, N_v = 64, v_{\max} = 8, \Delta t = 0.01$.

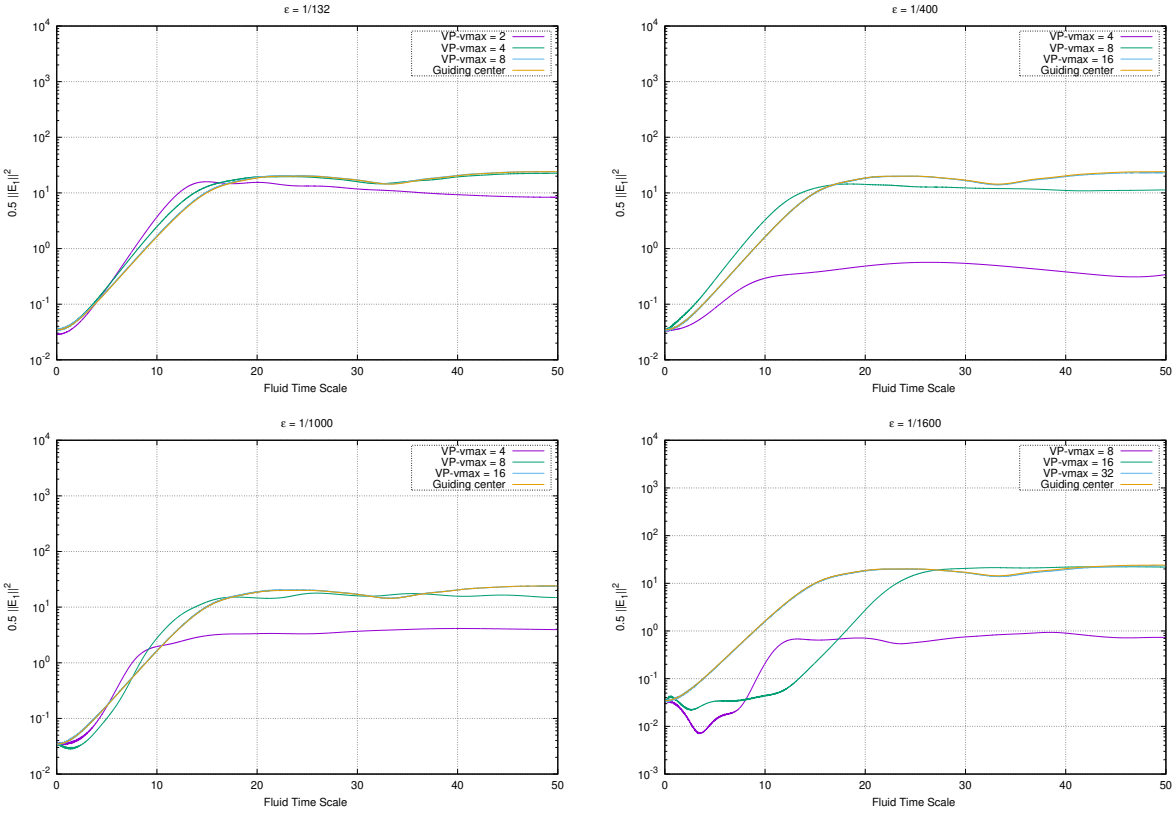


Figure 6: The time evolution of electrostatic energy in the first dimension under strong magnetic field with Scovel's splitting. $N_x = 128, \Delta t = 0.01$.

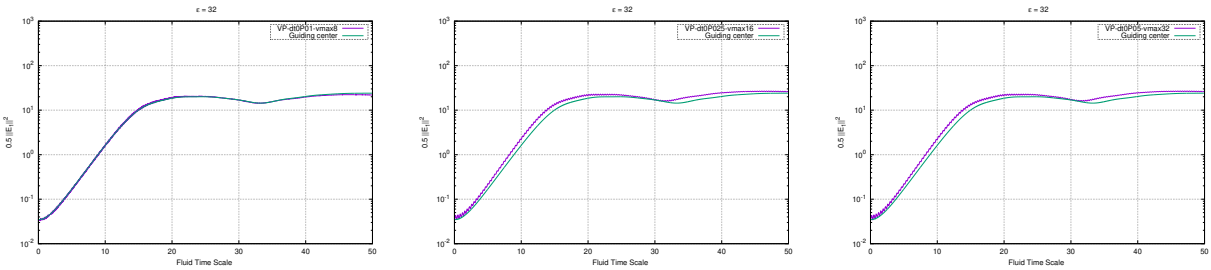


Figure 7: The time evolution of electrostatic energy in the first dimension under strong magnetic field with Scovel's splitting. $N_x = 128$. From left to right we plot the $\frac{1}{2}\|E_1\|_2^2$ at $\Delta t = 0.01$, $\Delta t = 0.025$, and $\Delta t = 0.05$.

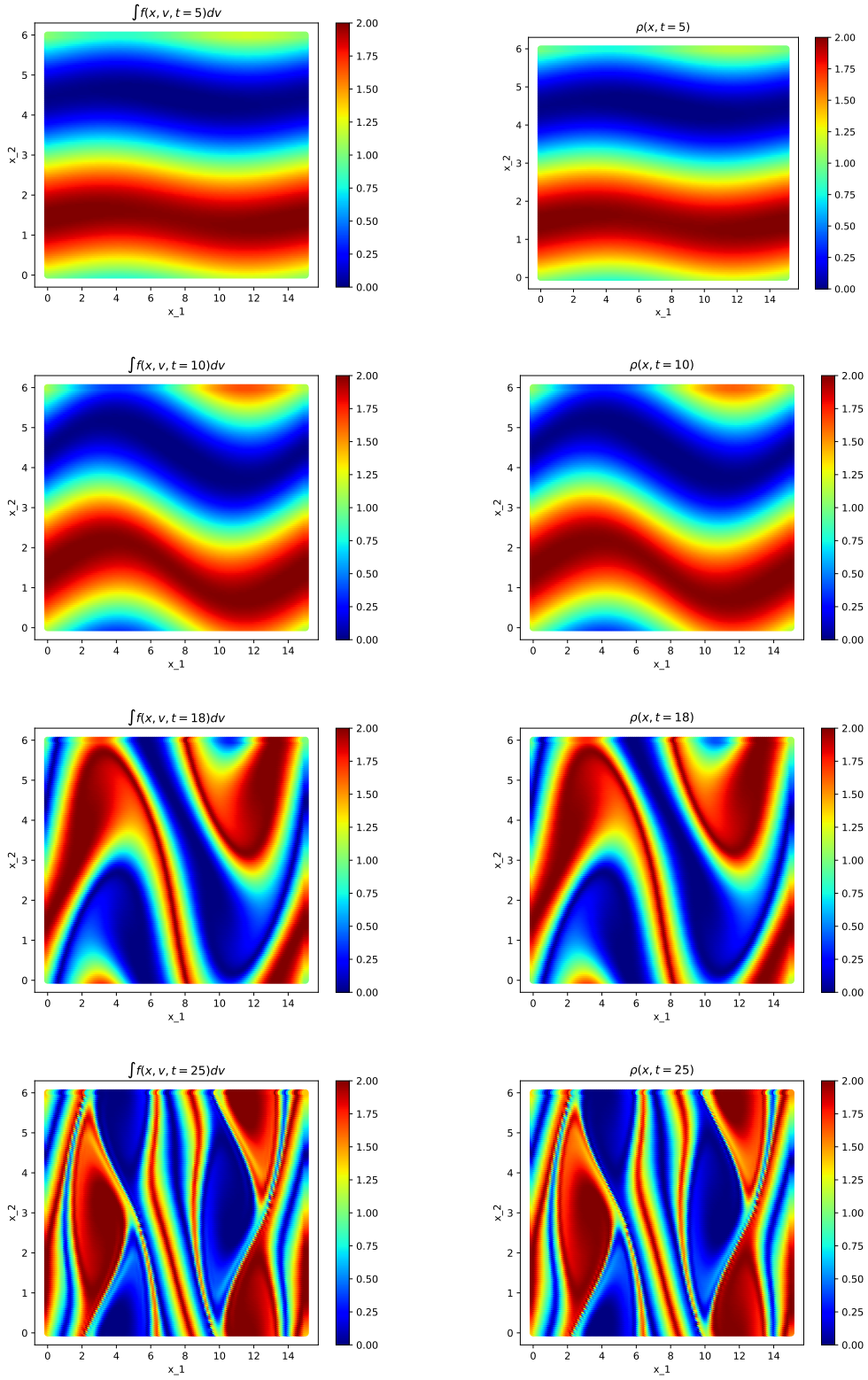


Figure 8: Simulation for the time evolution of the density of the Vlasov-Poisson system with $\varepsilon = 10^{-4}$ (left) and of the guiding center model (right). $N_x = 128, N_v = 32, \Delta t = 0.1$.

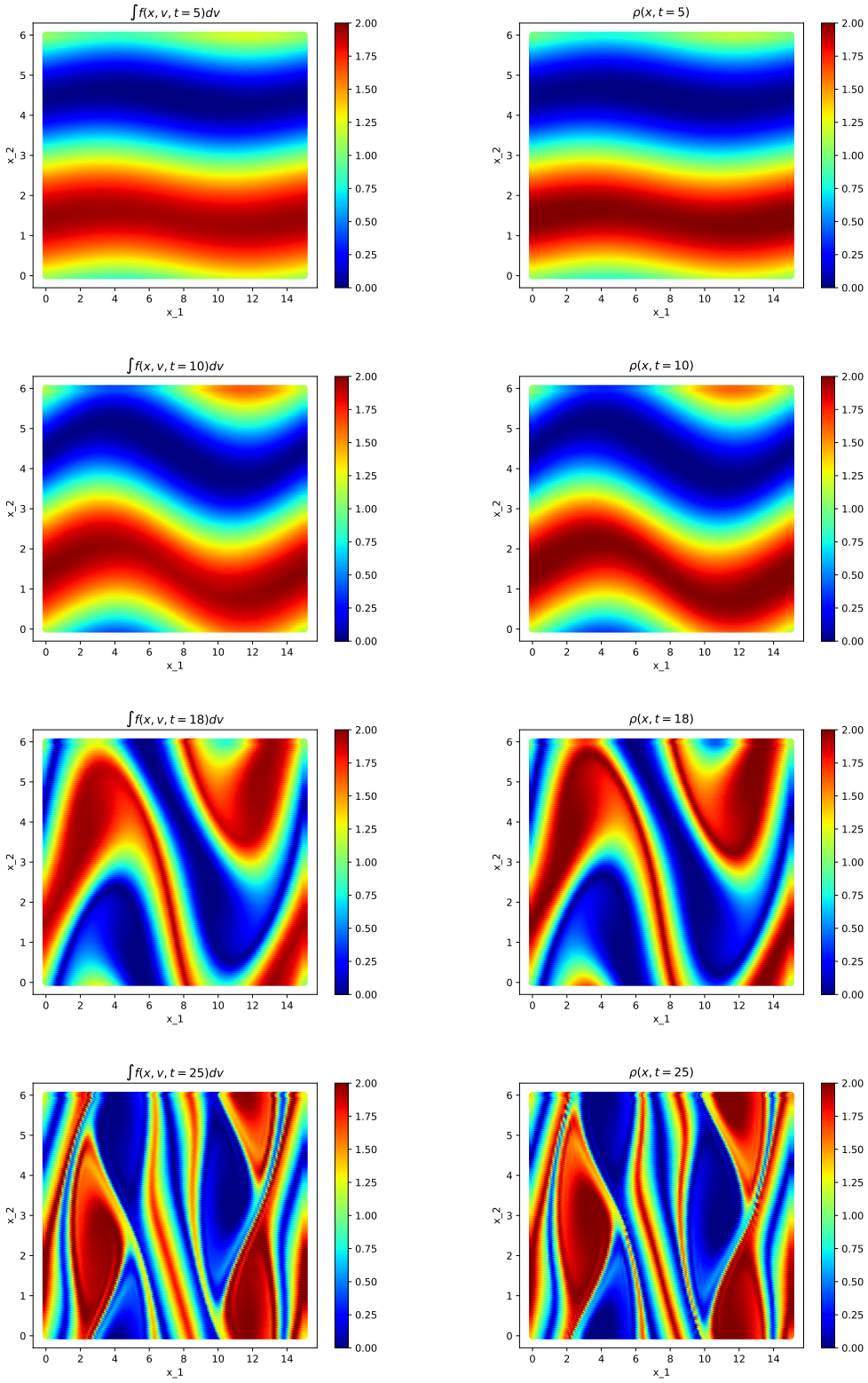


Figure 9: Simulation for time evolution of the density of the Vlasov-Poisson system with $\varepsilon = 0.01$ (left) and of the guiding center model (right). $N_x = 128, N_v = 32, \Delta t = 0.01$.

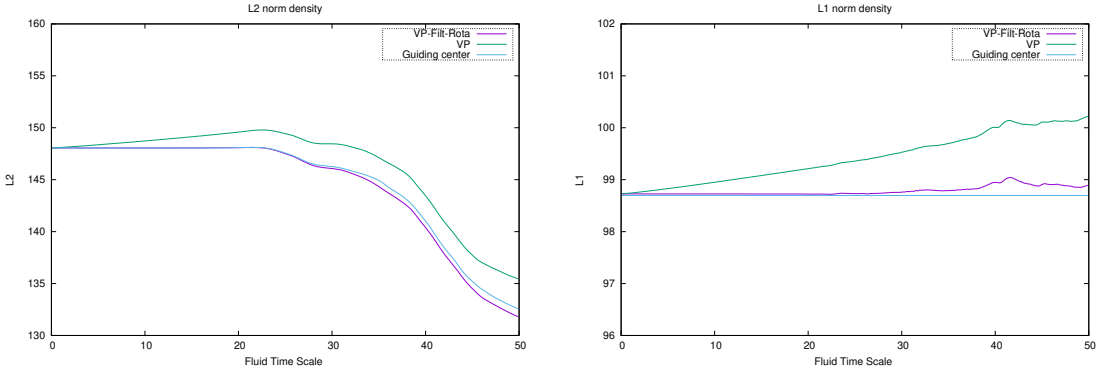


Figure 10: Comparison between the time evolution of theoretically quantities of the Vlasov-Poisson system with $\varepsilon = 10^{-4}$ and the guiding center model. $N_x = 128, N_v = 32, \Delta t = 0.1$.

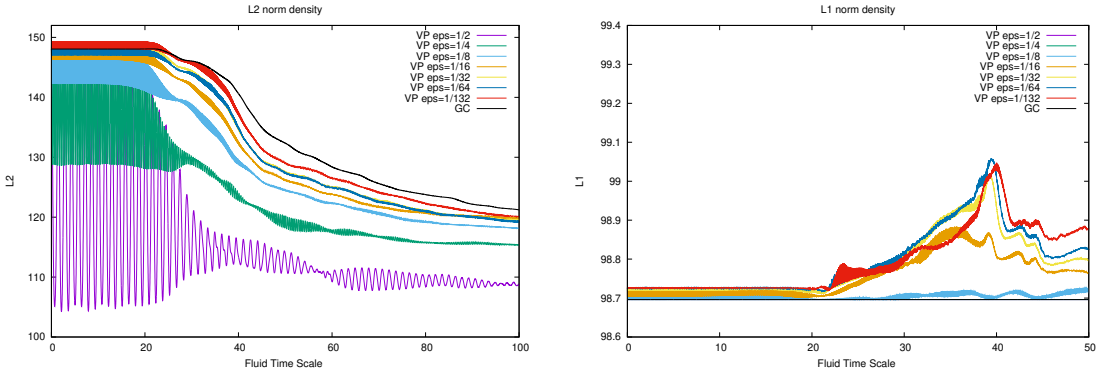


Figure 11: Comparison between the time evolution of theoretically quantities of the Vlasov-Poisson system with several values of $\varepsilon$ and the guiding center model. $N_x = 128, N_v = 64, v_{\max} = 8, \Delta t = 0.01$.

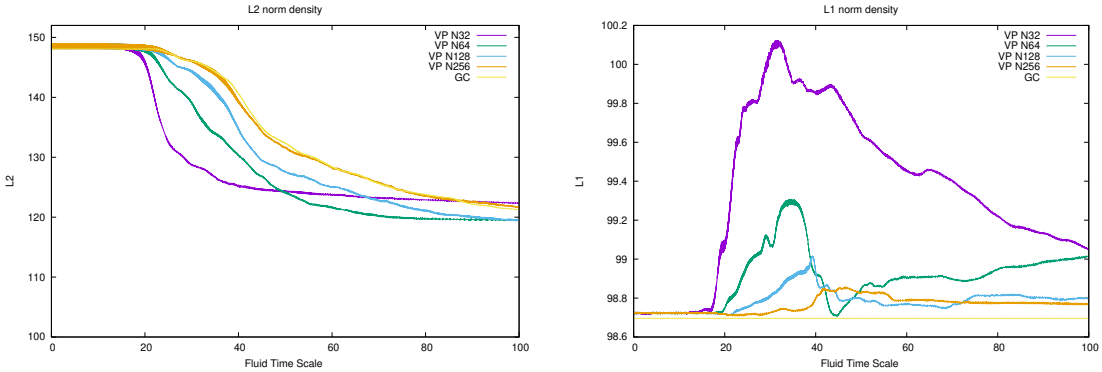


Figure 12: Comparison between the time evolution of theoretically quantities of the Vlasov-Poisson system when $\varepsilon = 1/32$ with several values of $N_x$ and the guiding center model with $N_x = 128$. $N_v = 64, v_{\max} = 8, \Delta t = 0.01$.